A critical review: Recent advances in "digital" biomolecule detection with single copy sensitivity

Haomin Liu [a,**], Yu Lei [a,b,*]

[a] *Department of Chemical and Biomolecular Engineering, University of Connecticut, Storrs, CT, 06269, USA*
[b] *Department of Biomedical Engineering, University of Connecticut, Storrs, CT, 06269, USA*

A B S T R A C T

Detection of a single biomolecule, ranging from nucleic acids, proteins, viruses to bacteria, is of paramount importance in various fields including biology, environment, food and agriculture industry, public health, and medicine. With the understanding of the biological functions of these biomolecules (or bioparticles) and their impacts on public health, environmental pollution, and food safety, advanced detection techniques are unprecedentedly demanded for their early and/or sensitive detection. In this critical review, a series of elegant research about digital detection of biomolecules with potential single copy sensitivity is reviewed and summarized with the focus on the design principle and the innovation of how to accomplish the "digital" detection concept. Starting with a brief introduction on the importance of digital detection, recent advances in "digital" biomolecule detection with single copy sensitivity are grouped and discussed based on the difference of signal reporting systems, including surrogate signal development for "digital" detection, direct visualization for "digital" detection, and nucleic acid amplification enabled "digital" detection. Interdisciplinary combination and integration of different cutting-edge techniques are also discussed with details. The review is closed with the conclusion and future trends.

1. Introduction

Biomolecules (or bioparticles), ranging from nucleic acids, viruses to cells, are important analytical targets in various fields including biology, environment, food, public health, and medicine. Biomolecules consist of a big family that can exist in different forms (e. g., deoxyribonucleic acid (DNA)/ribonucleic acid (RNA), protein biomarkers, viruses, cells) with a dimension spanning from nanometers to micrometers. Therefore, the detection methods of biomolecules may vary and can be classified based on the nature of the targets. For example, recent outbreak of coronavirus disease 2019 (COVID-19) pandemic is an infectious disease caused by severe acute respiratory syndrome coronavirus 2 (SARS-CoV-2, an RNA virus) and thus different methods have been developed for COVID-19 based on the nature of target molecule (Thompson and Lei, 2020): The biomolecule that used to diagnose COVID-19 in the gold standard of Reverse Transcription Quantitative Polymerase Chain Reaction (RT-qPCR) is a segment of viral RNA (January et al., 2020), while the biomolecules targeted in serological immunoassays are viral-specific antibodies (Immunoglobulin M

and Immunoglobulin G) (Long et al., 2020). Besides, the intact virus particle can also be a potential target molecule in COVID-19 detection. In another example, *Escherichia coli* (*E. coli*) O157:H7, one of the Shiga-like toxins-producing bacteria, is a pathogen that must be detected in raw milk and undercooked ground beef for food safety (Gally and Stevens, 2017; Karch et al., 2005). Furthermore, p24 capsid protein, a component of the human immunodeficiency virus (HIV) particle, is a biomarker for the diagnosis of the HIV in an early stage (Barletta et al., 2004). With the understanding of the biological functions of these biomolecules (or bioparticles) and their severe impacts on public health, advanced detection techniques are unprecedentedly demanded for their early detection. For instance, the concentration of p24 capsid antigen in HIV- patients infected within the first two weeks ranges from 50×10^{-18} M to 15×10^{-15} M (Barletta et al., 2004). If this concentration range could be detected accurately, the diagnosis of HIV could be achieved at its earliest stage which could benefit to early and effective treatment. However, most of current methods can only measure concentrations higher than 10^{-12} M, and thus are not able to offer the required sensitivity for early diagnosis (Giljohann and Mirkin, 2009).

* Corresponding author. Department of Chemical and Biomolecular Engineering, University of Connecticut, Storrs, CT, 06269, USA.
** Corresponding author.
  E-mail addresses: haomin.liu@uconn.edu (H. Liu), yu.lei@uconn.edu (Y. Lei).

Therefore, to develop advanced sensing platforms with superior sensitivity and accuracy becomes a frontier in the diagnosis of biomolecules.

The main obstacles hindering current detection methods toward ultra-sensitivity include the sluggish development in sensing principles and limited resolution of instruments. In 1993, real-time PCR was first presented, which opened the door to nucleic quantification with high sensitivity (Higuchi et al., 1993), while since the early 1990s, the emergence of bead-based ELISA has promoted the immunoassay considerably (Son et al., 2018), Also, the blossom of microfluidics boosted particle detection through all fields (Baker et al., 2009; Sakamoto et al., 2005). Currently, polymerase chain reaction (PCR), enzyme-linked immunosorbent assays (ELISA), and colonies forming units (CFU) counting on plates are gold standard methods for qualification or quantification of nucleic acids, proteins, and bacteria, respectively. All of them belong to ensemble tests which typically require sufficient target particles or reporter molecules to generate a measurable signal as readout (Scheme 1). However, as the numbers of target molecules decrease, the magnitude of the signal decreases accordingly, which is not measurable after being below the resolution of current instruments. The past decades have been witnessing significant progress in the aforementioned methods. Nevertheless, progress still lags behind the need for ultra-sensitivity at the single copy level due to the use of the same principles as in ensemble tests. Therefore, a transformative revolution, instead of increment improvement, is required toward this end. Consequently, to replace precedent ensemble tests with "digital" tests and then enable the detection of a single biomolecule either directly or indirectly has been attracting more and more attention.

The fundamental principle of single bioparticle detection is to isolate individual biomolecules and develop and detect the signal from every single biomolecule, followed by counting the total numbers of them to calculate the concentration. The difference between ensemble and single bioparticle detection can be illustrated in Scheme 1. The most common strategy employed in the latter one is to physically compartmentalize individual bioparticles into a small volume, detect the signal from each one, and then count the total numbers. Other strategies include introducing a surrogate such as an enzyme, a fluorophore or a bead that can establish a one-to-one correspondence between a surrogate and an individual biomolecule, and then monitoring the activity or event related with the individual surrogate such as enzymatic reaction, fluorescence, and bead mobility, followed by statistical analysis to illustrate the concentration of biomolecules. Compared with convectional ensemble detection strategies, "digital" detection of biomolecules can accomplish a much higher sensitivity because every single bioparticle as an end-point entity can be detected in principle. Besides, the acquisition of the results is straightforward and not complicated which can avoid cumbersome data analysis and eliminate the potential errors associated with data processing or bulk detection. Explorations on single-particle

detection have been a continuous effort and numerous advancements have been accomplishing by embracing new sensing concepts since 2010. In this critical review, a series of seminal reports about single-biomolecule detection systems for nucleic acids, proteins, viruses, and bacteria are reviewed and summarized with the focus on the design principle and the innovation of how to accomplish the "digital" detection concept. Moreover, recent advances in "digital" biomolecule detection with single copy sensitivity are grouped based on the difference of signal reporting systems, including surrogate signal development for "digital" detection, direct visualization for "digital" detection, and nucleic acid amplification enabled "digital" detection. Interdisciplinary combination and integration of different cutting-edge techniques are also discussed with details. Finally, the review is closed with the conclusion, remarks, and future trends.

## 2. Surrogate signal development for "digital" detection

The size of small biomolecules such as proteins is usually at a scale of several to tens of nanometers. Such a small size is difficult to be directly detected by current instruments. Therefore, to establish surrogate amplification systems for targeted small biomolecules is an indispensable goal in the development of the entire detecting platform. Up to date, a series of surrogate amplification systems have been developed, including enzyme-catalyzed system, bead-labeling system, and fluorophore conjugation system. In this section, seminal surrogate amplification systems that are specifically applied for single-molecule detection are summarized.

2.1. Single molecule array (SiMoA)

To develop a simple, accurate, rigorous "digital" detection method, multiple steps are typically included such as entrapping only one molecule of interest in a small chamber, introducing a measuring tool to detect it, and counting and adding the number of chambers containing individual molecules. In 2010, a new method named digital ELISA (dELISA) relying on the SiMoA achieved "digital" biomolecule detection employing enzyme-catalyzed colorimetric system (Rissin et al., 2010), The invention of this method can be regarded as a milestone in ELISA since it transforms traditional ensemble ELISA (detecting analog signal) to a dELISA (detecting digital signal).

The principle of this method is to compartmentalize every single immunocomplex in a small chamber and then count the number of chambers that contain the target molecule. In this method, the structure of the immunocomplex adapts the conventional beads sandwich structure (Fig. 1a), in which each target molecule binds with capture antibodies functionalized magnetic beads and biotinylated detection antibody. Enzymes that can generate a color/fluorescence change of the substrate for signal detection are conjugated with streptavidin that can tightly bind with biotins on the detection antibody. This conjugated reporter molecule is also a part of the immunocomplex. To prevent multiple target molecules from binding with one capture antibodies labeled magnetic bead, excessive beads is added to guarantee there are only unreacted beads and immunocomplexes containing only one target molecule. This bead solution is then loaded into a 50 fL chamber (Fig. 1b). This small chamber can only trap either one bead or nothing. After beads loading, the enzyme substrate is added into each well and a silicone gasket is utilized to seal chambers to prevent evaporation. The products of the substrate catalyzed by the enzyme are fluorescent. Under the fluorescent microscope, only chambers contain immunocomplex show fluorescence (Fig. 1c and d). Counting and adding the number of fluorescent chambers and other beads included chambers without fluorescence signal enable the calculation of the target molecule concentration.

The three crucial steps guarantee the success of this method, including the formation of immunocomplexes containing only one target molecule, selection of a proper beads' concentration, and
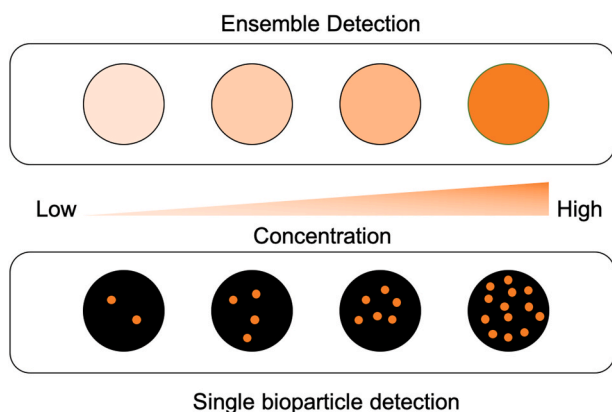
Scheme 1. The difference between ensemble and single bioparticle (or biomolecule) detection.
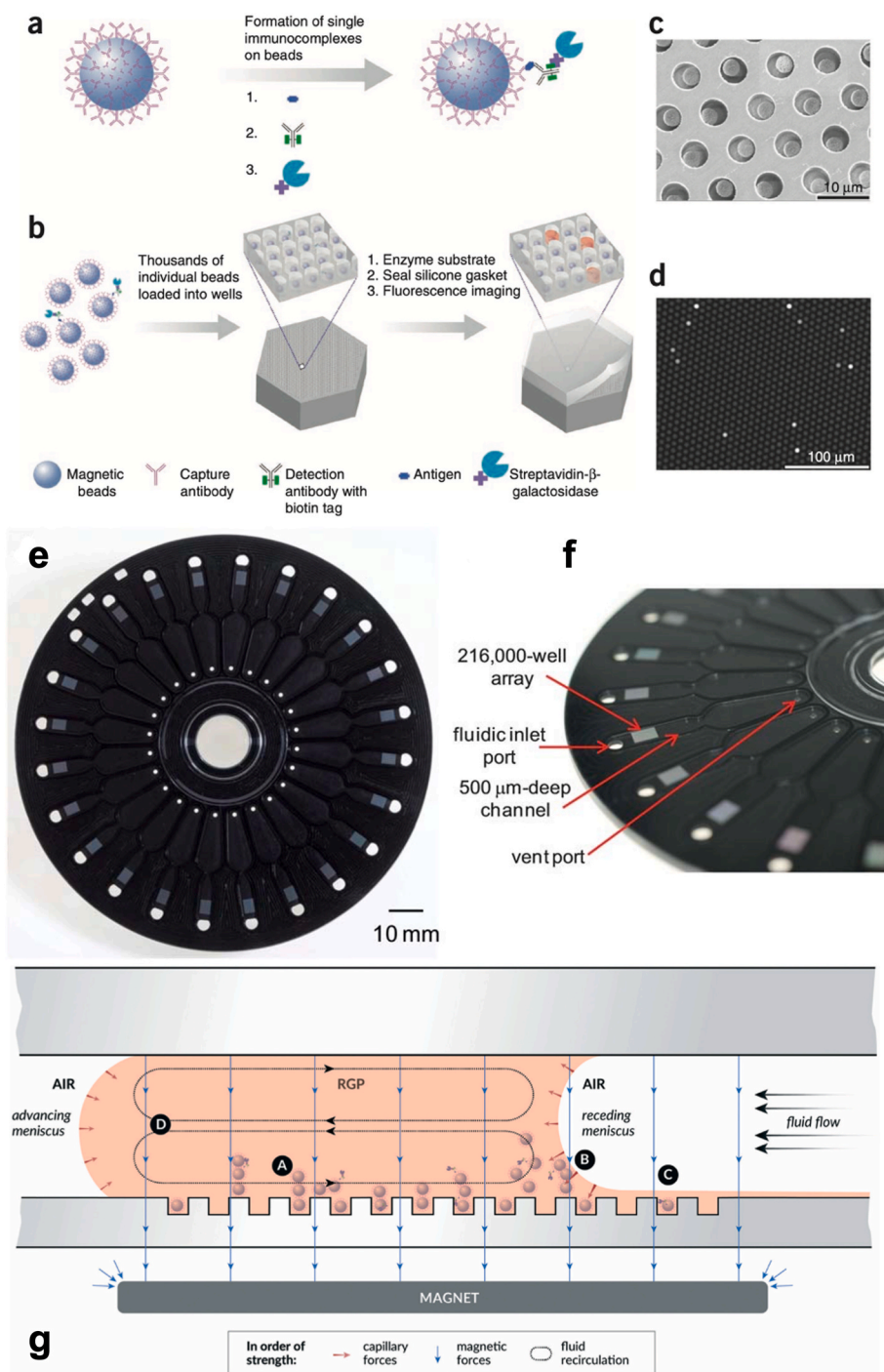
Fig. 1. (a) Formation of immunocomplex; (b) Beads loading; (c) Scanning electron microscope (SEM) image of chambers with and without beads; (d) Fluorescent image of the array. Reprinted with permission from (Rissin et al., 2010). Copyright 2010 Springer Nature Limited. (e) A photograph of a disk device with 24 array assemblies arranged radially. (f) Details of channel features. Reprinted with permission from (Kan et al., 2012). Copyright 2012 The Royal Society of Chemistry. (g) The scheme of MMS. Reprinted with permission from (Kan et al., 2020). Copyright 2020 The Royal Society of Chemistry.

fabrication of a small volume chamber. The secret of forming immunocomplexes containing only one target molecule is to reduce the ratio of beads to target molecules. When the ratio of target molecules to capture antibodies labeled beads is smaller than 1:1, Poisson distribution (Eq (1)) can be used to compute the percentage of beads that contain a single immunocomplex (Rissin et al., 2013a).

$$P_k^\lambda = \frac{e^{-\lambda} \times \lambda^k}{k!} \tag{1}$$

P_k^λ represents the probability of conjugating k molecules to one bead, while λ represents the average number of target molecules on one bead. For example, the concentration of target molecules is 10 aM and the

volume of the solution is 100 μL, thus there are 602 target molecules in total. If 40,000 beads are employed to capture these molecules, λ is equal to 602 divided by 40,000, which is 0.01505. The possibility that each bead captures only one target molecule (k = 1) is $P_1^{0.01505}$, which equals to 1.48%, and $P_0^{0.01505}$ (beads capture nothing) is 98.51%, and thus the summarization of remained possibilities from where k equals to 2 and larger is around 0.01% that can be ignored. This calculation indicates that the one-to-one correspondence of the bead and target molecule is possible, thus laying down the foundation for the SiMoA system. Furthermore, the determination of proper bead concentration used in the experimental operation is crucial for maintaining the high reliability of this method. First, the number of beads must be sufficient to capture target molecules to satisfy thermodynamic and kinetic requirements.

From a thermodynamic perspective, beads with enough numbers guarantee the high capture efficiency beyond the protein-antibody equilibrium. From a kinetic perspective, an appropriate concentration of beads allows the diffusion of target molecules in a reasonable time to reach immobilized antibodies. Second, the number of beads must be sufficient to overcome Poisson noise, which means there are enough beads trapped into chambers and enough positive chambers to be detected. Third, both excessive and deficient numbers of beads could lead to the failure of experiments. Excess of beads increases the background noise because of nonspecific binding, thus decreasing the accuracy of the detection, while an inadequate number of beads lose the capture efficiency. Also, the small volume of the chamber for trapping is indispensable for signal detection. The configuration of the immunocomplex only allows one streptavidin conjugated with one or several reporter enzymes to be bound. The fluorophores produced by such small numbers of enzymes are undetectable if the volume of the chamber is too large. In contrast, the fluorescent product can be condensed by reducing the volume of the reaction chamber, which enables the signal to be differentiated from the background and detected by the instrument. Besides, the small volume guarantees only one immunocomplex rather than two or more to be confined, which is also one of the foundations for the accuracy of SiMoA.

Prostate specific antigen (PSA) and tumor necrosis factor alpha (TNF-α) in 25% sera have been employed to validate the SiMoA system. The limit of detection (LOD) is around 50 aM for PSA and 150 aM for TNF-α, respectively. The clinic sample from patients undergoing radical prostatectomy has also been tested with a concentration of 0.4 fM to assess its applicability for clinical samples. Although SiMoA is elegant and the prototype (a glass fiber bundle containing 50,000 chambers) is utilized as the compartment device, the fabrication of this device is expensive and cumbersome, which prevents this technique from wide utilization. To improve the commercialization capability, a sample loading disk (Fig. 1e and f) has been designed as the substitute for a glass fiber bundle. Batch production of this device can be achieved by using the injection moulding process used in digital versatile disc (DVD) manufacturing (Kan et al., 2012). This device also accomplished multiplexed single molecule immunoassays in 2013 (Rissin et al., 2013b). In the same year, an automated device (secure digital reader) has been integrated to achieve automatic detection of dELISA (Nie et al., 2014). In 2018, a competitive immunoassay was also developed employing this platform (Wang et al., 2018).

To further improve the sensitivity, each step of this analysis was systematically assessed and optimized, and a new generation platform named low bead digital ELISA was developed in 2020 (Kan et al., 2020). The key step causing bead loss is "beads loaded and sealed in microwells". Thus, the new beads loading method named magnetic-meniscus sweeping (MMS) was introduced as a substitute, which improves the sensitivity down to the sub-attomolar level. As illustrated in Fig. 1g, a stationary magnet is placed under the microwell. The magnetic force pulls and vertically chains magnetic beads. Partial magnetic beads are directly wrapped into the microwells. The remained ones are chained vertically or free in the solution. Following several cycles of back and forth flowing, capillary forces at the receding meniscus would destroy the chained structure and drive these remained beads into microwells. However, unavoidable bulk fluidic forces have negative effects, leading to aggregation and recirculation of the beads. It is a competition between the two positive drive forces and the negative ones, which may require more studies to clarify which process could gain the upper hand. After replacing the standard loading method with the MMS, Interleukin (IL)-17A has been used as a representative biomolecule to assess the loading efficiency. The bead loss has been significantly reduced from 88.6% to 39.1%. The LOD has been lowering down to 0.7 aM.

Up to date, this technique has been commercialized for nearly 7 years. Target molecules that can be detected including bacteria (Song et al., 2013), antibodies (Gaylord et al., 2015a), various biomarkers (Gaylord et al., 2015b; Janelidze et al., 2016; Khalil et al., 2020; O'Connell et al., 2020; Rivnak et al., 2015; Wu et al., 2015), and gene

expression (Yan et al., 2016). In 2020, this dELISA was applied to perform the COVID-19 antibody test that can detect antibodies at 1000 × lower concentrations. More theoretical considerations (such as kinetic, optics, etc.) behind the design of this platform can be found elsewhere (Chang et al., 2012; Dinh et al., 2016; Vo-Dinh et al., 2014).

2.2. Droplet-based compartmentalization for "digital" detection

The microfluidic technique is powerful in the generation of droplets with a small and well-controlled volume. This merit has been successfully employed to confine one single immunocomplex in one droplet. Thus, such compartmentalization enables individual target molecules to be detected and counted to determine the concentration. In 2013, a reusable microfluidic device, integrated with fluorescent microscopy, was developed to accomplish single PSA molecule detection (Shim et al., 2013).

The principle to accomplish single molecule detection by microfluidic technique is simple. As illustrated in Fig. 2a–c, droplet flow is comprised of droplets with a volume between 5 and 50 fL which are called femtodroplet. Because of the tiny volume, each droplet can only contain one or zero enzyme (β-galactosidase) labeled immunocomplex, composed of capture antibodies labeled bead, target molecule, and reporter enzyme-labeled detection antibody. The solute in the droplet solution is fluorescein-di-β-D-galactopyranoside (FDG) which can be hydrolyzed by β-galactosidase. The released products glowing green fluorescence can be detected using a fluorescent microscope. Because this fluorescent signal development requires about 10 min, a storage area (Fig. 2b) is inserted in the flow pathway. Within the storage area, multiple trap zones are utilized to store the femtodroplets temporally. After signal development and recording, those droplets are flushed out (Fig. 2d–g) and the device is ready to receive the next batch of samples for analysis.

The design principle of this platform is easy to understand. The most fundamental and essential requirement is to generate the droplet with a small volume at the femtoliter level. In the present study, the strategy to generate femtodroplets is to shear water with immiscible oil, a process relying on large shear force and low surface tension. A locally narrow flow-focusing nozzle is introduced in this system to produce a large shear force, while the solution is premixed with a surfactant to reduce the tension of the oil-water interface. Another parameter optimized is the flow rate which controls the frequency of droplets generation to determine the volume of an individual droplet. A confocal optic setup is employed to measure the frequency which must be over a million hertz to guarantee the droplet volume at a femtoliter level.

PSA has been selected as a representative target molecule to evaluate the performance of this platform. The LOD is 46 fM (1.2 pg/mL), which is nearly 2 orders of magnitude better than conventional ELISA. One highlight of this study is the reusability of the hardware, comparing to single-use microfluidic devices. However, the main limitation and complexity encountered in all other microfluidic methods are still not overcome.

2.3. Droplet-free digital ELISA

To compartmentalize every single immunocomplex into a small droplet is one of the most popular strategies employed in digital detection/counting. Because of the complexity of the compartmentation process (e.g. the requirement of customized sample holders or specific design of a microfluidic system), more convenient methods are desperately needed. In 2016, a droplet-free platform was devised and integrated with a tyramide signal amplification (TSA) system (Akama et al, 2016, 2019b).

TSA strategy and signal detection employing flow cytometer are the core of the design. Similar to commonly used bead-based sandwich ELISA, the structure of an immunocomplex in this sensor is comprised of capture antibody labeled magnetic beads (diameter, 2.8 μm), target

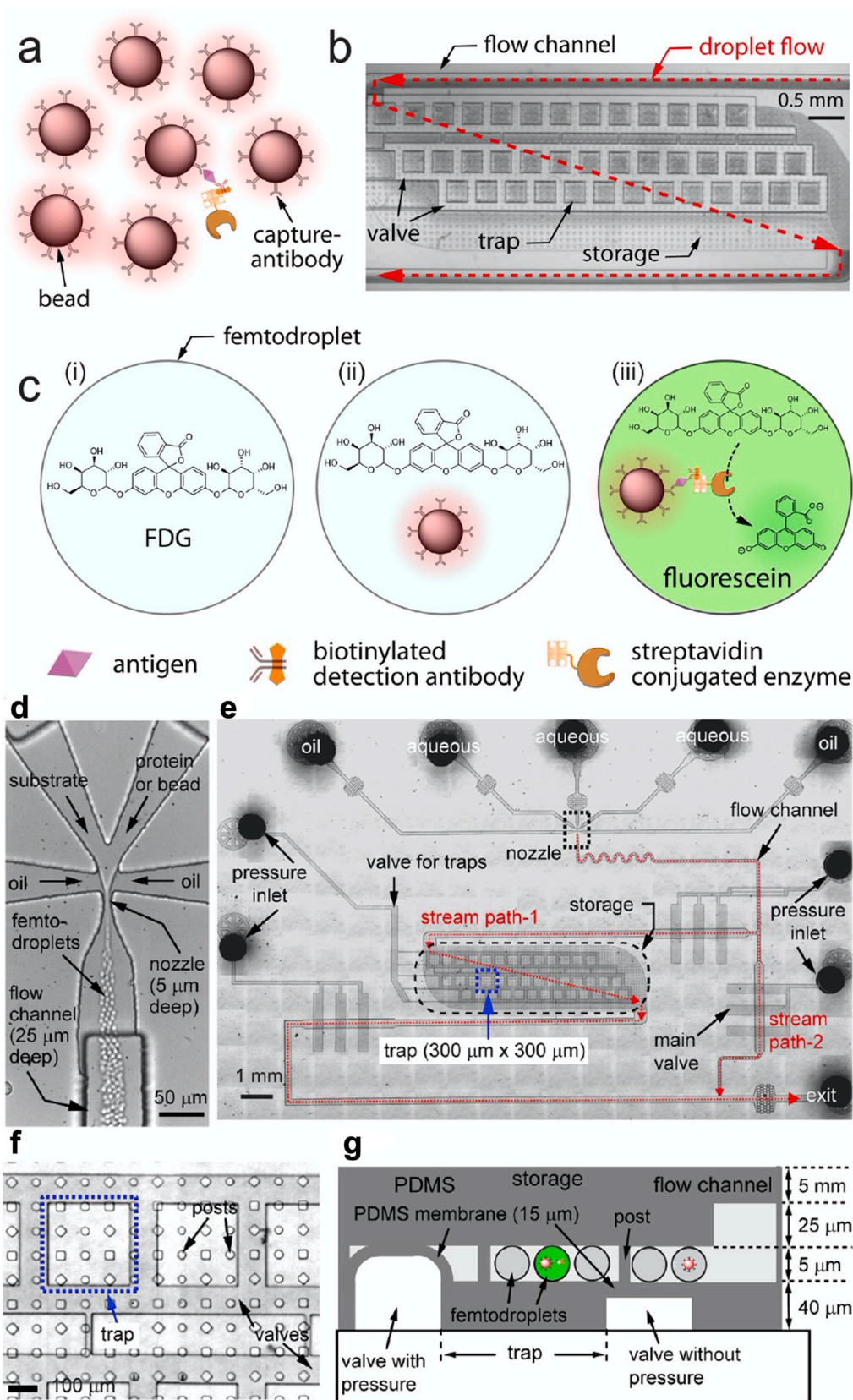**Fig. 2.** Principle of microfluidic droplet-based single molecule detection (a–c). Details of the microfluidic device (d–g). Reprinted with permission from (Shim et al., 2013). Copyright 2013 American Chemical Society.

molecule, biotinylated detection antibody, and streptavidin labeled horseradish peroxidase (HRP) conjugation (Fig. 3a). To enable immunocomplexes to be detectable, biotinylated tyramide solution mixing with hydrogen peroxide is added in the immunocomplex solution. HRP in the immunocomplex converts tyramide into the tyramide radicals, which can bind to aromatic moieties on the surface of all adjacent proteins including capture and detection antibodies, target molecule, and streptavidin. The addition of streptavidin-labeled fluorescent dye endows the immunocomplex labeled with fluorescein, and thus amplifies the signal (Fig. 3e). As a comparison, there is no fluorescence in the free magnetic beads. The fluorescein-labeled beads in the mixture solution are then tracked and counted using flow cytometry to calculate the concentration of the target molecule. As the signal amplification strategy is self-recognized, only the HRP labeled immunocomplex can bind with reporter molecules, thus eliminating nearly all false-positive signals for improved accuracy. Also, the flow cytometer is one of the most commonly used instruments in a biological lab, which provides high accessibility to the users to carry out the detection.

There are two significant considerations in this design to assure the assay accuracy: optimizing the ratio of beads to target molecules and preventing tyramide radical from cross-reacting with free capture antibody labeled beads. In this study, the concentration of capture beads must be at least 10 times larger than that of target molecules. Otherwise, the one-to-one correspondence between one bead and one target molecule cannot be maintained when the ratio is at a low level. In other words, more than one target molecule can bind to one capture beads, which can smash the final results completely. Another potential issue is that tyramide radicals might not only bind to the corresponding adjacent immunocomplex, but also free capture antibodies labeled beads. If occurred, there would be enormous false positive signals, which disqualify the conclusion. According to the results in the paper, this phenomenon was not observed during the experiments. One possible explanation is that the lifetime of tyramide radicals is too short. There is no enough time for these radicals to diffuse and react with other particles far way, rather than the adjacent ones.

Hepatitis B surface antigen was employed as a model target biomolecule to demonstrate the applicability of this platform. The LOD is as low as 139 aM, which is 20 times better than conventional ELISA. In 2019, a multiplexed assay for hepatitis B surface antigen and IL-6 mixture were developed and validated. In the multiplexed
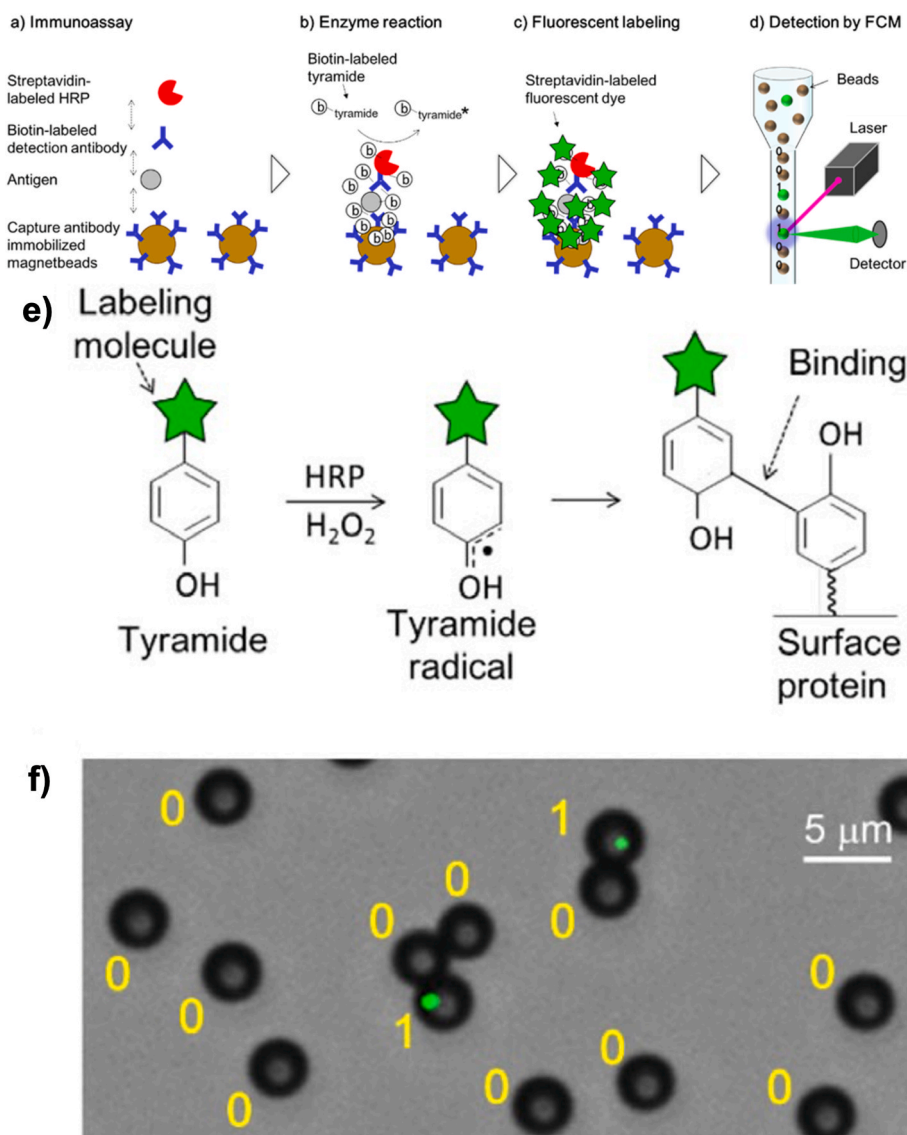

Fig. 3. The workflow of droplet-free dELISA based on a TSA system (a–d). Principle of the reaction of the labeled tyramide substrate with a surface protein (e). Overlay of fluorescent and brightfield images. 0 and 1 represent negative and positive signals respectively (f). Reprinted with permission from (Akama et al., 2019b). Copyright 2018 Wiley Periodicals, Inc.

measurement, the LODs for hepatitis B surface antigen and IL-6 are 20 fM and 4.8 fM, respectively. The LOD increase in multiplexed assay study might be attributed to the increase of the background noise associated with the nonspecific absorption between different antibodies (Akama et al., 2019b).

2.4. Reporter elution enabled "digital" detection

Unlike immunocomplex compartmentalized dELISA requiring delicate separation devices, other methods avoiding the isolation and compartmentalization of each immunocomplex have been emerging in the past decades. An advanced dELISA introducing elution of detection reporter and evaporated particle sedimentation was developed recently (Zhang et al., 2020).

The principle of this dELISA method is similar to the conventional beads-based sandwich ELISA (Fig. 4A and B). Capture antibody functionalized magnetic beads are mixed with antigens. The ratio of capture

beads to antigens is larger than 10:1 to ensure that either one or zero antigen can bind with one single capture bead. Bovine serum albumin (BSA) blocking was employed to eliminate the non-specific binding. After the binding of antigen on capture beads and BSA blocking, excessive detection antibody functionalized polystyrene spheres (DPS) are added to form immunocomplexes, followed by magnetic-assisted separation to remove excessive DPS. Particles remained are the immunocomplexes and the free capture beads. The number of immunocomplexes is equal to that of DPS (bound with immunocomplexes). Thus, DPS can be regarded as the detection reporter. To collect the DPS for analysis, an acidic buffer is added to decompose the immunocomplex. After the dissociation of the sandwich structure, a magnet is utilized to fix the magnetic capture beads and free DPS in the solution are eluted three times for subsequent evaporated particle sedimentation. Within every elution, the DPS solution is loaded into the customized chamber and the liquid is entirely evaporated and the number of DPS is imaged by an inverted microscope. The number of the DPS, representing the
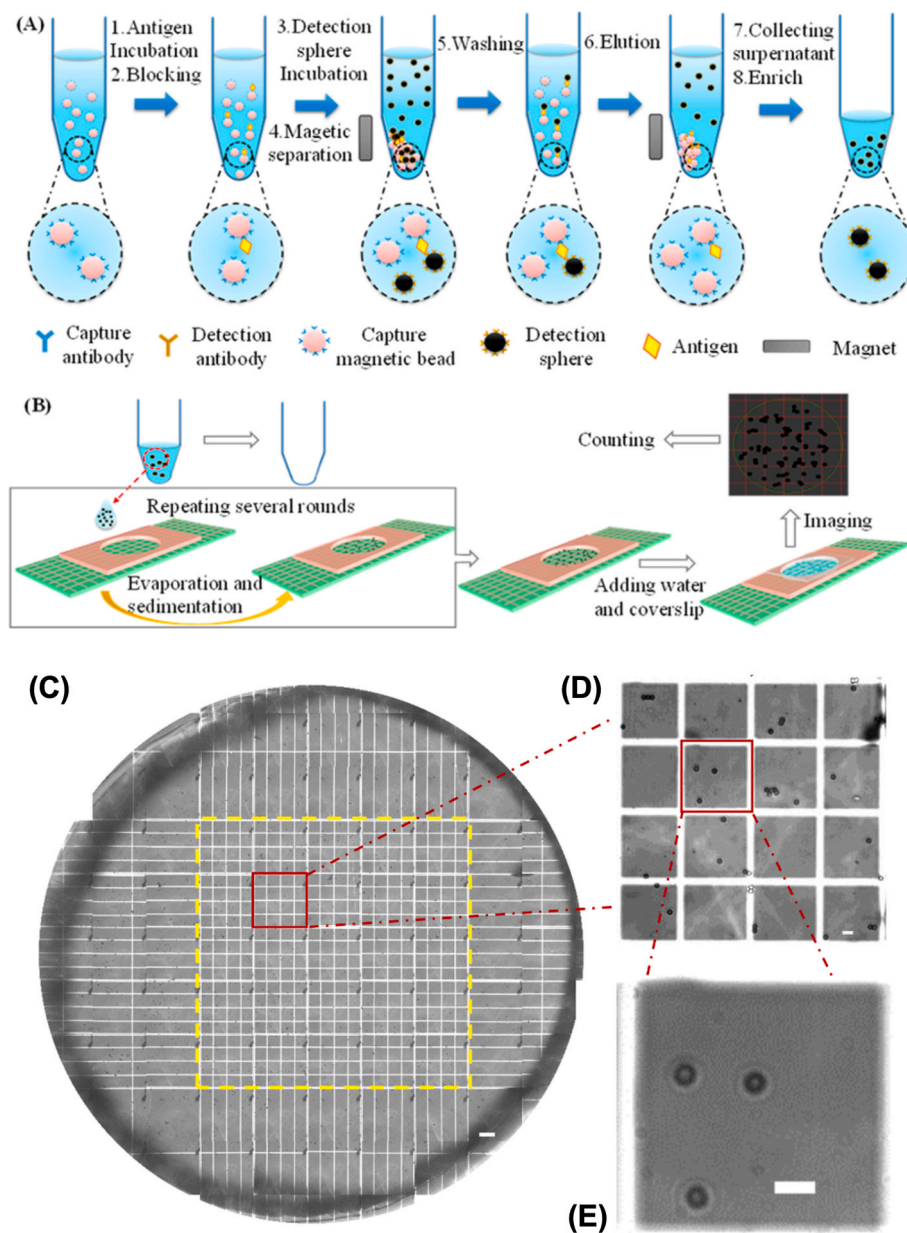

Fig. 4. Scheme of digital counting ELISA. (A) Formation of Immunocomplexes and the disassociation of the detection reporters; (B) Evaporated particle sedimentation process; (C) Stitched images of the entire chamber bottom. (D) and (E) details of zooming in a small area. Reprinted with permission from (Zhang et al., 2020). Copyright 2019 American Chemical Society.

concentration of the antigen, is counted.

Although the sensing principle is not complicated, this method requires optimizations of a series of crucial parameters to guarantee success. The first parameter to be considered is the bead functionalization. On one hand, the amount of the antibody must be high enough to cover the entire surface of the beads. On the other hand, the ratio of functionalized beads to the antigen must be larger than 10:1. This is due to the consideration of the kinetics in the antibody-antigen binding reaction (Chang et al., 2012). The second parameter is the size of the DPS which is essential for digital counting. Free DPS incline to aggregate and form the cluster. If the size is too small, it is difficult to distinguish the clusters from individual DPS under low magnification which is used to collect images. In this study, the diameter of the DPS employed is 3.0 μm. This diameter is large enough for an individual DPS to be discerned from the clusters under $40 \times$ magnification. The number of washing time and elution time is the third parameter which must be controlled within an appropriate range. For washing, one-time washing can wash out 50% of free DPS. Theoretically, the more wash times, the more accurate final results. However, with the increase of washing time, the immunocomplexes begin to disassociate, which reduces the accuracy of detection. It is a tradeoff between washing times and accuracy. In this study, the best number of washing time is three times. For elution, the more elution times, the more opportunities for capture beads to escape into the eluant. Thus, the number of elution times is three to generate the best results.

Except for the optimization of the aforementioned crucial parameters, three innovative design considerations in this platform are also essential for reliable detection. The first one is to add an elution step in the protocol to detach the DPS. Most of the dELISA employ the complete sandwich immunocomplex as the detection entity. A potential drawback is that the complete immunocomplex limits the flexibility of subsequent processes considerably. Extra attention must be paid to maintain its complexity, which is inconvenient for the operation. The introduction of the elution perfectly circumvents this problem. Such elution step also enables the utilization of the subsequent evaporated particle sediment, which is the second innovation in the design. Evaporation at 90 °C allows the sample size to be small, thus resulting in the captured image as small as possible. The elution is incubated on a hot plate until all the liquid is evaporated. This delicate design not only accelerates the speed of eluant addition but also achieves the DPS enrichment. The third innovation in the design is that the bottom of the substrate glass is patterned with square grids (Fig. 4C-E). This design facilitates the operators to capture the image of the entire area frame by frame.

Carcinoembryonic antigen (CEA) was employed as a model target to evaluate this dELISA platform. The dynamic range can be determined from 5×10^{-18} to 5×10^{-16} M and the LOD is 4.9×10^{-18} M. Two clinical plasma specimens were also tested, and the results showed negligible deviation from the actual values, indicating the high reliability of this platform.

2.5. "Cocktail" separation system enabled "digital" detection

The procedure of an ELISA experiment is always tedious because it requires multiple reaction steps to form the multi-layered immunocomplexes and considerable washing steps between each reaction step. These washing steps play a crucial role to mitigate nonspecific binding for a more accurate result. For instance, there are 100 immunocomplexes to be detected, but 100 nonspecific reporter-labeled detection antibodies are also in the well due to non-specific binding. The final result obtained would be overstated. Although washing steps can mitigate the influence of nonspecific binding, a potential negative impact of multiple washing steps is to destroy the immunocomplex, especially at a low concentration of target molecules. When the number of immunocomplexes is low, the antibody and the antigen tend to dissociate with each other as the free or nonspecific antibodies are washed out, thus resulting in understated counting numbers. Therefore, the washing step

could interfere with the performance in ultrasensitive "digital" detection. In 2018, a multipath technology-based digital imaging platform was developed to accomplish the digital counting concept (Gite et al., 2018). The highlight of this platform is that it circumvents washing steps through a unique design.

The introduction of a density gradient medium, OptiPrep, is the secret to circumvent washing steps during the formation of immunocomplexes. OptiPrep is a reagent commonly used for the isolation of cells and subcellular organelles. The density of OptiPrep solution is slightly bigger than that of water, indicating that two phases with an interface could form once loading water on the top of the OptiPrep solution (like a cocktail). The microwell employed in the detection is pretreated with a solution with two solutes including OptiPrep and then dried to develop a cushion. In the detection, the beads-based ELISA is utilized. Magnetic bead whose density is higher than both water and OptiPrep solution is functionalized with capture antibodies. Fluorescent beads (the reporters) that can be suspended in water are functionalized with detection antibodies. As illustrated in Fig. 5b, the mixture of antigen and excessive antibody labeled beads are added into the pretreated microwell in a one-pot manner, which also re-constitute the cushion. After the reconstitution of the cushion layer and the formation of the immunocomplexes, there is an OptiPrep layer at the bottom of the microwell. On top of the OptiPrep layer, it is the solution containing immunocomplexes and free magnetic and fluorescent beads. Among the three components, immunocomplexes are the desired particles to be collected. Free fluorescent beads must be excluded for signal interference. Free magnetic beads are useless but do not influence subsequent operation. To collect the immunocomplexes without free fluorescent beads, a magnet is placed beneath the microwell, and both immunocomplexes and free magnetic beads are pulled into the OptiPrep layer. Density difference facilitates immunocomplexes and magnetic beads to remain in the bottom layer after removing the magnet and also prevents free fluorescent beads to enter the OptiPrep layer. Employing this innovative design, this platform successfully completes the separation without using washing steps and also decrease the turn-around time.

After optimization of the immunocomplex separation, MultiPath imaging technology is developed to achieve the digital count without magnification. As illustrated in Fig. 5a, a light source is utilized to glow the fluorescent beads in immunocomplexes sitting on the bottom of the microwell. The excited beads emit photons that are collected by the lens and photons emitted from each fluorescent bead generate one white pixel dot in the recording images for counting (Fig. 5c). One potential issue of this imaging strategy is how to avoid interference from free fluorescent beads in the top layer because both layers are transparent and the light source can also excite the fluorescent beads in the top layer, but the signal from the top layer is undesired. To address this issue, a black dye, another solute co-existed in the pretreated solution, is employed to block light penetration through the OptiPrep layer after the reconstitution. Not to use magnification in detection is another merit of this platform, because of the one-to-one correspondence among immunocomplex, fluorescent bead, and the white dot on the image. This is not only enlarging the imaging area but also simplifying the imaging process compared with other digital counting techniques relying on sample compartmentalization.

By employing this platform, *Clostridium difficile* toxin B in stool samples has been successfully detected with a LOD of 45 pg/mL and a wide dynamic range covering four to five orders of magnitude (Gite et al., 2018). A standard method, cellular cytotoxicity neutralization assay, was also conducted as a reference for comparison. The new platform shows considerable sensitivity, specificity, and accuracy. The turn-around time of this technology is only half an hour, which is faster than the leading homogenized ELISAs (Eastwood et al., 2009; Pollock et al., 2015).
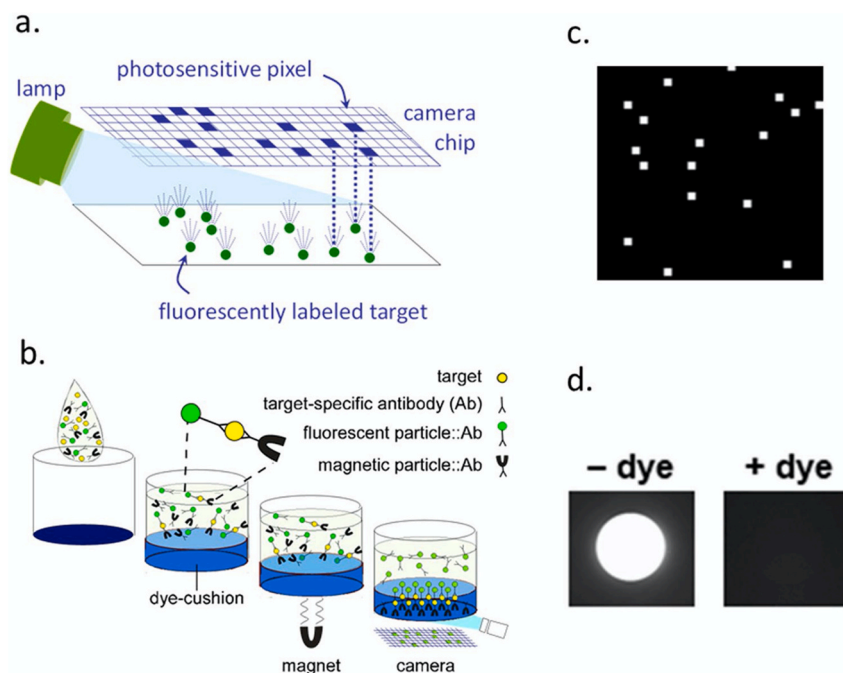
Fig. 5. (a) Mechanism of digital imaging. (b) Scheme of wash free immunoassay. (c) A non-magnified image. (d) Images of well with and without dye that is employed to eliminate background noise. Reprinted from (Gite et al., 2018) under the Creative Commons Attribution 4.0 International License http://creativecommons.org/license s/by/4.0/.

2.6. *"Digital" biomarker sensing enabled by particle mobility (BPM)*

Brownian motion is one of the most common phenomena when particles are suspended in a fluid. Those particles tend to collide with other molecules within the system irregularly. It is apparent that the mobility of the particles must be restricted partially once they are immobilized or tethered. This mobility difference was successfully employed as a detection parameter to continuously monitor the target at an individual molecule level (Visser et al., 2018).

To achieve continuous monitoring, the design of tethered immunocomplex generates different mobility activities from alternately interchanged bound and unbound states. A tethered immunocomplex is illustrated in Fig. 6a, which is modulated from the conventional bead-based sandwich ELISA. Magnetic beads (diameter, 1 μm) and supporting substrates are functionalized with capture molecules and detection molecules, respectively. Once target molecules are added, sandwich immunocomplexes are constructed through immunoreactions. Therefore, magnetic beads are tightly tethered to the substrate by a double-strand DNA, which restrains the beads to only move within a certain area. This restraint always exists whether the immunocomplex formed or not. As adding the target molecules into the capture beads tethered substrate, two different situations appear. If there is no immunocomplex formed, the pattern that appeared on the images captured by the dark-field optical video microscope is an irregular dot spreading circle (Fig. 6b). Upon the formation of the immunocomplex, the pattern transfers to spindle shape on the periphery of the circle. These two patterns represent two states of the molecules, which are named bound and unbound state correspondingly. Under a microscope, bound and unbound state alternately appears rather than a constant single one (Fig. 6c), which can be attributed to the reversibility of the affinity reaction, especially at a low target concentration. At a low target concentration, target molecules more likely to disassociate with capture and detection molecules, indicating that the lifetime of the unbound state is longer than the bound one. As an opposite, target molecules tend to form immunocomplex with the increase of the number of the target molecules, thus resulting in a decrease of the unbound state lifetime. At a certain concentration of the target molecules, the lifetimes of the two states have a unique value (Fig. 6d). That is how to achieve concentration detection by measuring single molecule activity continuously.

Single strand DNA (ssDNA), thrombin, and ssDNA in undiluted blood plasma were employed as target molecules to challenge this design. For instance, 501 particles were tracked to obtain the bound (7.3 ± 0.1 s) and unbound (63.8 ± 0.4 s) state lifetime for 62.5 pM of ssDNA. For 3.125 μg/mL thrombin, 407 particles were tracked to calculate the lifetime of the two states, 9.3 ± 0.1 s for the bound state and 113 ± 2 s for the unbound state. A series of concentrations were then tested to establish the lifetime-concentration curve with sensitivity down to picomolar and nanomolar level. The sensor also shows certain reusability, but the performance is not as good as the first-time use after washing and reloading. For the two molecules tested, the reusability for ssDNA detection is better than for thrombin because of the interaction of thrombin immunocomplexes are more stable and harder to be destroyed without damaging the biomolecules. These studies indicate that this platform can be employed to monitor single molecule activity with high sensitivity, accuracy, and specificity. Although only ssDNA and thrombin were tested, the structure designed here is easy to be adapted to other target molecules that can form sandwich immunocomplexes such as aptamer, antibody fragments, and virus. The high affinity of target molecules and the corresponding antibodies ensure the high specificity. Also, the selection of the beads (diameter, 1 μm) guarantees the digital readout of the signal. Compared with the nanometer-sized biomolecule, the bead is relatively large and, consequently, the steric hindrance allows only one target molecule binding with the detection molecule rather than several target molecules binding with one bead. Moreover, this technology is self-contained and no other reporter such as fluorophores and amplification chemistry are required, which further improved the accuracy.

3. Direct visualization for "digital" detection

The ideal scenario for accurate and precise particle detection is to directly observe particle of interest without using any functionalization or reporting system, as any extra operations may cause unnecessary damage or loss of the particles themselves. Also, direct observation/
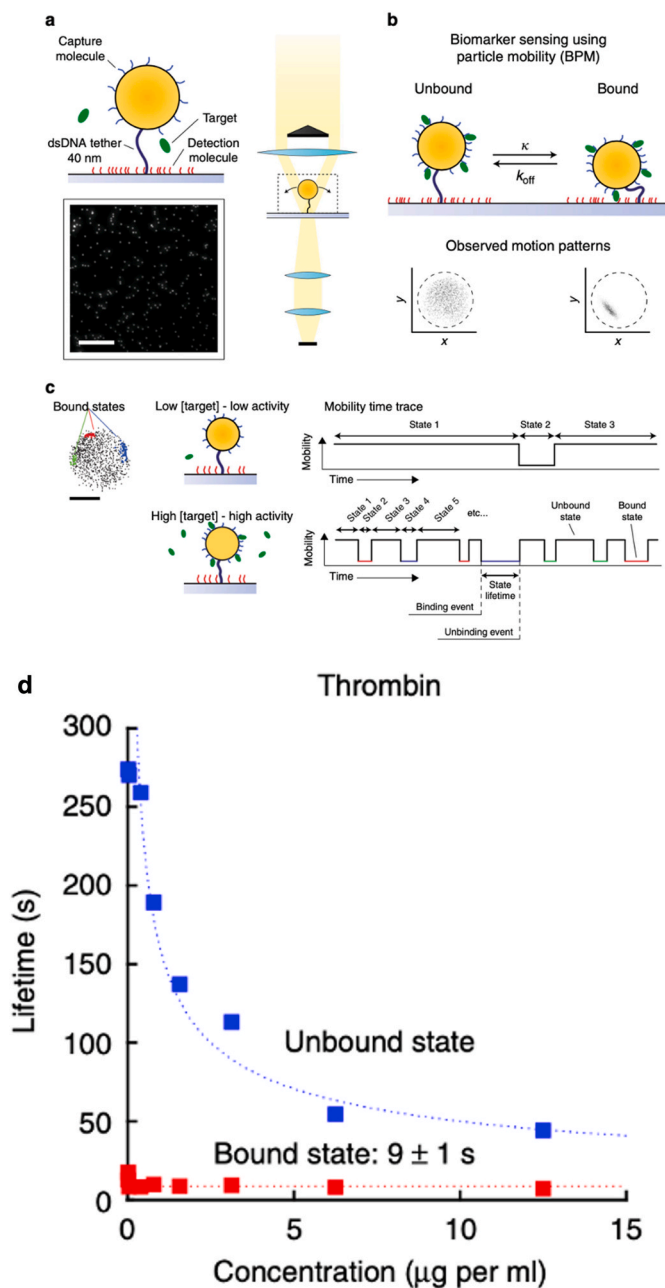
Fig. 6. Sensing principle of the biosensor using particle mobility (a–c). Dependence of lifetimes of the bound (red) and unbound (blue) states on the thrombin concentration (d). Reprinted from (Visser et al., 2018) under the Creative Commons Attribution 4.0 International License http://creativecommons.org/license s/by/4.0/. (For interpretation of the references to color in this figure legend, the reader is referred to the Web version of this article.)

visualization can simplify the entire operation procedure as well. In this section, four studies focusing on virus and bacteria detection through digital visualization are summarized.

3.1. Surface plasmon resonance imaging (SPRi) enabled "digital" detection

Since its invention in 1988, SPRi has become a powerful tool in two-dimensional imaging of small particles such as DNA and proteins in a label-free manner (Phillips et al., 2006; Rothenhäusler and Knoll, 1988; Shumaker-Parry et al., 2004). However, the intrinsic constraint of the

traditional SPRi instrument (prism-based plasmon excitation) leads to a poor spatial resolution, thus greatly limiting its application. To overcome this barrier, SPRi using a high numerical aperture (NA) microscopic objective was successfully developed in 2007 (Huang et al., 2007). This breakthrough facilitates a single virus to be detected and characterized in 2010 (Wang et al., 2010).

The principle of high NA SPRi is illustrated in Fig. 7a, as the p-polarized monochromatic light passes through the objective and reaches the interface of gold and glass in a total internal reflection (TIR) mode, evanescent waves are produced (Zhou et al., 2020). At the same time, the surface plasmon polaritons (SPPs) also propagate along the interface originated from the free electrons of gold. Once the frequency of the SPPs and that of the evanescent wave are equal to each other, conditions to maintain TIR disappear and the decay reflection emerges. This decay can be monitored and recorded by the charge-coupled device (CCD) camera. Images captured simultaneously are utilized for the following analysis.

The high NA SPRi platform is similar to the total internal reflection fluorescent microscope, but two minor modifications of modular elements enable it to be unique and advanced. One modification is to employ a pellicle beam splitter to replace the conventional dichroic mirror. This replacement circumvents interference patterns created by the turnings within the reflection path using the conventional splitter. The other is to introduce the high NA objective to replace the previous rotational angle scanning mode with linear motion of the stage, which optimizes the platform design and promotes the mechanical performance (Huang et al., 2007).

Digital detection for the virus was accomplished by employing the developed SPRi platform (Wang et al., 2010). Two different influenza
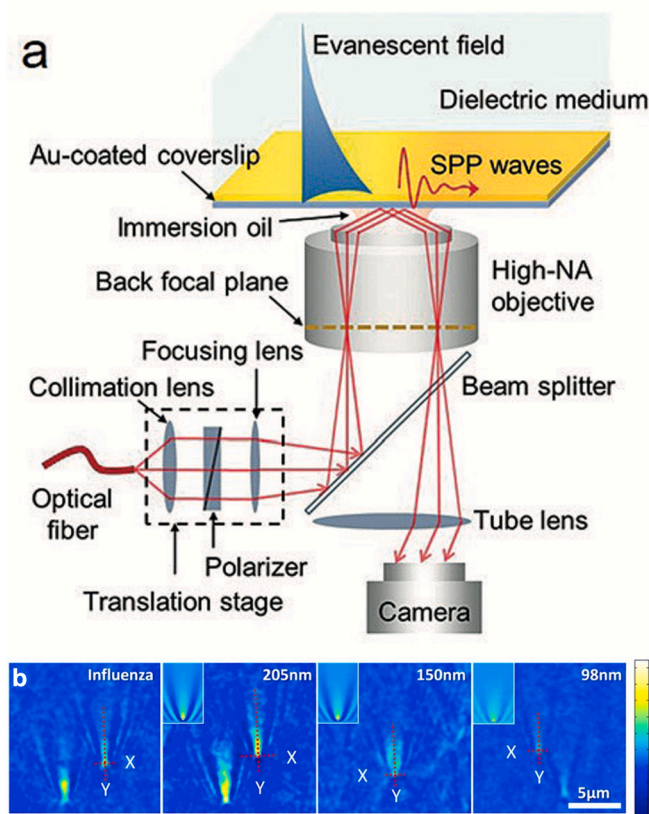

Fig. 7. (a) Principle of objective-type SPRi. Reprinted with permission from (Zhou et al., 2020). Copyright 2020 Wiley-VCH Verlag GmbH & Co. KGaA, Weinheim. (b) SPRM images of H1N1 influenza A virus and silica nanoparticles (Simulation results are inserts). Reprinted with permission from (Wang et al., 2010). Copyright 2010 National Academy of Sciences.

viruses and fixed-sized silica particles were imaged individually (Fig. 7b), and the diameter and mass of the viruses have been determined. For H1N1 Influenza A/PR/8/34, the diameter and mass are found to be 109 ± 13 nm and 0.80 ± 0.35 fg, respectively. For human cytomegalovirus, the diameter and mass are found to be 218 ± 10 nm and 6.5 ± 0.8 fg, respectively. This study offers an excellent tool in virus detection through direct visualization.

3.2. Continuous wetting films enabled "digital" detection

An axicon is a specialized lens within optics. It is widely employed as an element of the telescope and in laser eye surgery. Not limited to these common applications, a liquid axion lens-based particle detection platform was reported to achieve virus detection and size determination in 2013 (Hennequin et al., 2013).

To understand the principle of the platform, it is required to know the characteristics of an axicon. An axion is a lens with both a conical and a flat surface. Collimated light incident on the flat side is condensed first and then expanded into a ring. The resulting light is diffractive-free, which has been widely used in optics. However, the high intensity property of the resulting light is usually overlooked. Actually, this intensive resulting light can be captured and imaged to detect small particles. In this study, each target particle within a continuous film, dewetted polyethylene glycol (PEG) solution, forms an individual liquid axicon lens to condense incident light that can be collected to create images for analysis (Fig. 8a). A solution suspended with micrometer particles is loaded on the surface of the substrate. As the evaporation of the solvent, the solute is retained on the surface. PEG solution is then loaded to cover the entire specimen loading area and form a continuous wet film. During the naturally dewetting of the film, a bulk transparent thin layer that can be imaged is produced. Each individual particle forms a subtle bulge locally, which is treated as an individual liquid axicon lens. Every liquid axicon lens is imaged for analysis. Representative cross-section images of particles are shown in Fig. 8b and c.

Magnetic beads with 100 nm, 500 nm, and 1 μm were tested first and each size could be apparently identified. The size can also be correlated with local maximal intensity measured on the image (Fig. 8d–g). Cydia pomonella granulovirus (CpGV) and *Staphylococcus epidermidis* were further employed as target biomolecules to assess the performance of this platform. A mixture sample containing CpGV and *Staphylococcus epidermidis* bacteria was also successfully validated and the measured diameters were 330 ± 50 nm for CpGV and 0.7–1.3 μm for *Staphylococcus epidermidis*, respectively. Comparison with the size (0.5–1.0 μm) of *Staphylococcus epidermidis* from the literature indicates the high accuracy of the new technology (Schleifer and Kloos, 1975). The developed method could also be realized by utilizing lens-free on-chip imaging.

The liquid axicon lens-based platform possesses several advantages. First, materials and instruments employed in this platform are cost-effective and simple. Moreover, the large field of view (FOV) and the ability for lens-free on-chip imaging enable this platform to be a high throughput technology. However, the detection relies on the size, so the specificity cannot be guaranteed. Also, the extension of this method to the detection of smaller particles may be challenging, which may limit its application in protein biomarker detection.

3.3. Single particle interferometric reflectance imaging sensor (SP-IRIS)

The utmost barrier for detecting small biomolecules (e.g., viruses) through visualizing strategy is their smaller size comparing with bacteria and other cells. The small size results in both weak interaction with photons and low index contrast to the surrounding medium, which prevents these molecules from observing under the normal light microscopy. Recently, a new platform that overcomes this issue and achieves the visualization of small molecules was reported by introducing interferometry into the conventional optical system, namely SP-IRIS
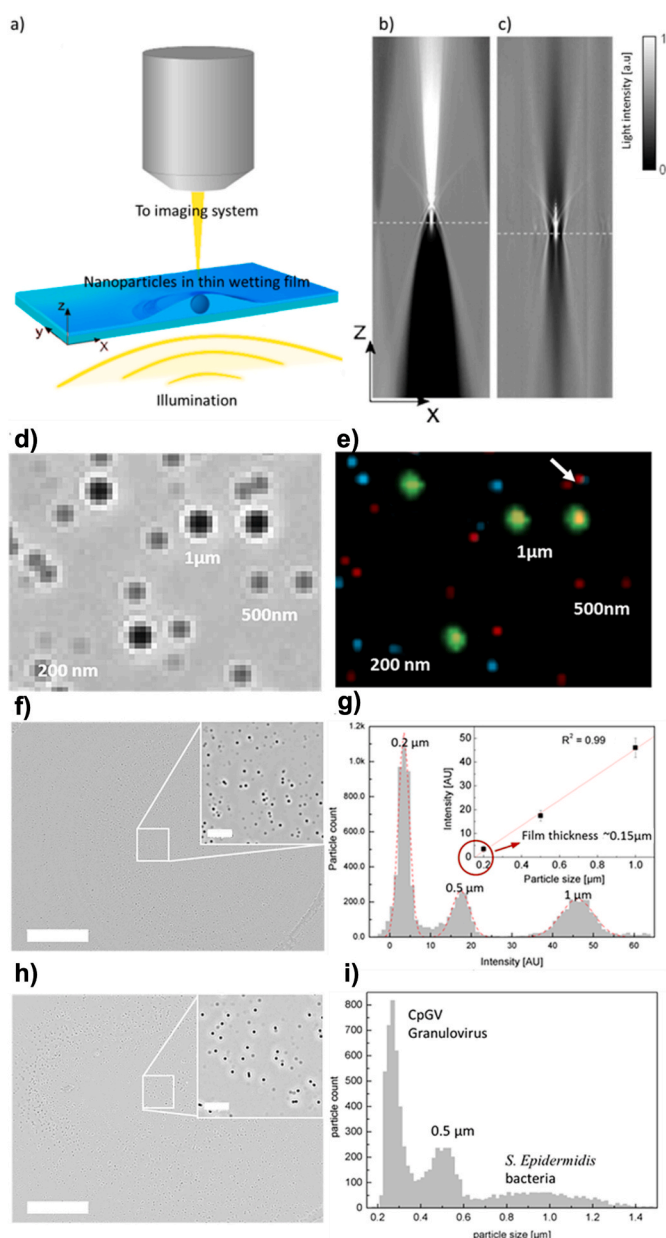

Fig. 8. (a) Scheme of the nanoparticles detected by axicon lens-based platform. (b) Image of the cross-section of a liquid axicon lens. (c) Image of the cross-section of a usual particle. (d) Bright-field and (e) fluorescent microscopic image of multiple sized magnetic beads sample. Within the fluorescent image, the diameters are 1 μm in green, 500 nm in red, and 200 nm in blue. Brightfield image of magnetic beads with 200 nm, 500 nm, and 1 μm in diameter. Scale bar is 1000 μm (100 μm for the inset). (g) Local maxima intensity distribution measured on the image (f). Brightfield of mixture sample including CpGV, ~1 μm *Staphylococcus epidermidis* bacteria, and 500 nm beads. Scale bar is 1000 μm (100 μm for the inset). (i) Local maxima intensity distribution measured on the image (h). The inner plot in (g) serves as the calibration curve to plot the maxima distribution as a function of the particle size Reprinted with permission from (Hennequin et al., 2013). Copyright 2013 American Chemical Society. (For interpretation of the references to color in this figure legend, the reader is referred to the Web version of this article.)

(Daaboul et al, 2010, 2014; Monroe et al., 2013; Reddington et al., 2013).

According to the classic quasi-static theory, nanosized particles can be regarded as induced dipoles describing signal strength of light scattered by them (Bohren and Huffman, 2008). Under this theory, the determined parameter of signal is the polarizability (α) of the small

particle, which is intrinsically determined by the radius (r) of the particle, following $\alpha \propto r^3$. Another parameter scattered electrical field (E_s), which is directly linked to the scattering intensity (I) of detection, is proportional to α, Thus, the correlation from particle to detection endpoint, $I \propto |E_s|^2 \propto \alpha^2 \propto r^6$, can be established. This relationship directly illustrates the reason why small molecules are unable to be visualized. For instance, if the radius of one particle decreases by 10-fold, the signal intensity decreases one million times, indicating that the intensity of the small particle is unable to be identified from the background noise. To overcome this limitation, the introduction of the interferometric system alters the regime of detection intensity, which is determined by E_s and the new reference electrical field (E_r) jointly.

$$I \propto |E_s + E_r|^2 = |E_s|^2 + |E_r|^2 + 2|E_s||E_r|\cos\theta \qquad (2)$$

where θ is the phase angle difference between the two fields. Within Equation (2), E_r and θ are two known parameters; E_s is far smaller than E_r, and thus it is negligible. Therefore, the interferometric system integrated detection intensity is proportional to r^3, which is amplified a thousand times than before. This signal amplification allows small particles to be detectable and visualized and thus enlarges both the dynamic range and the sensitivity of SP-IRIS based detection platform.

In 2010, SP-IRIS was fabricated to successfully detect individual nanoparticles and viruses with size for pathogen identification (Daaboul et al., 2010). The experimental platform is illustrated in Fig. 9A. A flat silicon dioxide layer whose thickness can be adjusted precisely is thermally grown on a smooth and uniform silicon substrate. When the particles are immobilized on the substrate, the scattered back-reflected light produces a quantitative interference signal which can be analyzed to obtain the size of particles. This platform is simple, chip-scaled, and reasonably priced, and a portable prototype designed for point of care was further reported in 2013 (Reddington et al., 2013).

To facilitate this platform to identify and size a single molecule, five decisive parameters (illumination wavelength, uniformity, NA, magnification, and camera pixel size) are optimized to obtain the best performance. A certain wavelength guarantees the highest sensitivity for particles within a certain range. As illustrated by Fig. 9B, the green LED (525 nm) is more sensitive than the red one (635 nm) once the particle size is below 100 nm. Uniform illumination is also required for size determination because the size of particles is calculated using the contrast of the central peak to surrounding background pixels. NA is another crucial parameter that directly affects the contrast between the particle and the background, while an appropriate magnification and camera pixel size play important roles in differentiating and isolating the particle from the background and overcoming the blur effect. In addition to the optimization of parameters above, several image processing techniques were applied to recognize the nanoparticle diffraction patterns in the image (Reddington et al., 2013). The utmost significant one is the scale invariant feature transform that can precisely localize the
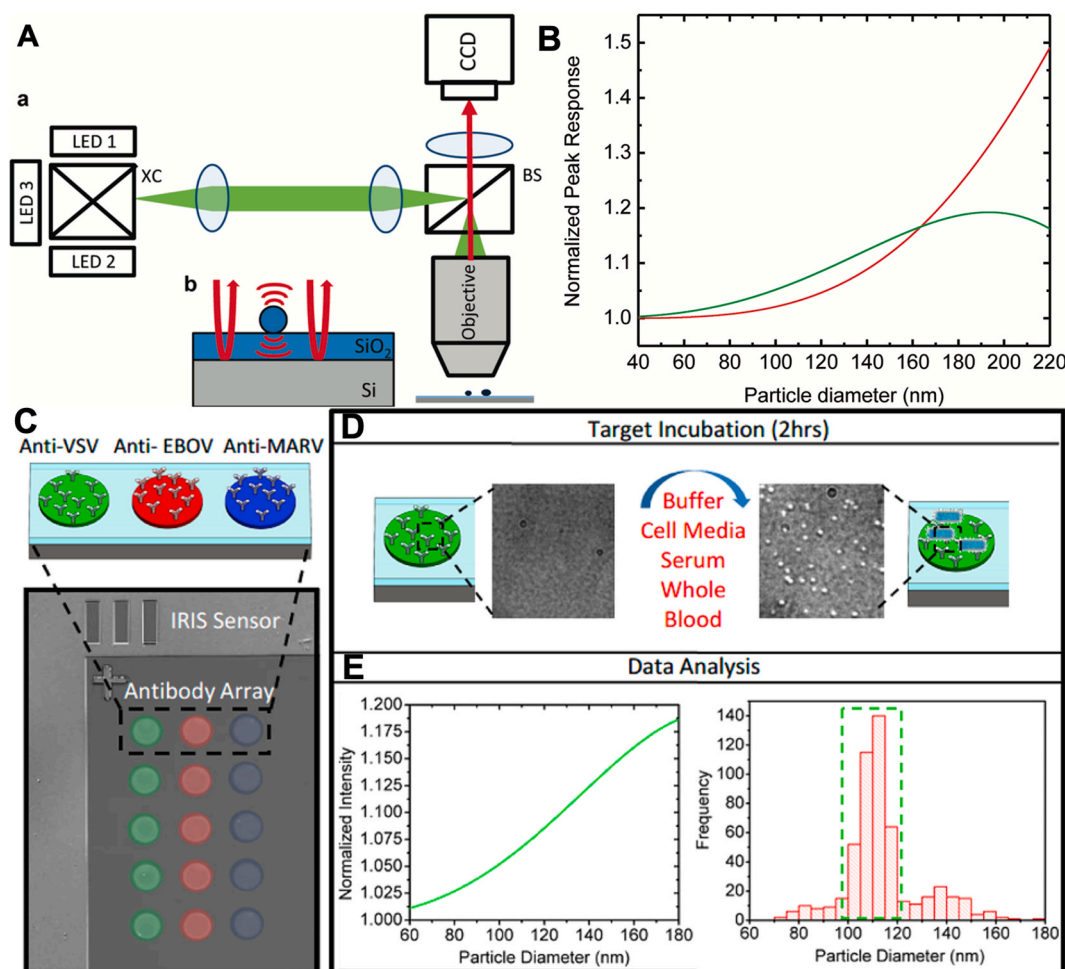

Fig. 9. (A) Experimental setup of SP-IRIS. a) Scheme of the optic setup where XC is a cube to combine beams from three different LEDs and BS is a beam splitter. b) Layered substrates with nanoparticles and interference signal produced. (B) Theoretical interference response versus particle size. The wavelength of the green cure is 525 nm and that of the red curve is 635 nm. Reprinted with permission from (Daaboul et al., 2010). Copyright 2010 American Chemical Society. (C) Configuration of the SP-IRIS. a) Arrayed chips with capture antibody; b) Virus capture; c) Data analysis. Reprinted with permission from (Daaboul et al., 2014). Copyright 2014 American Chemical Society. (For interpretation of the references to color in this figure legend, the reader is referred to the Web version of this article.)

nanoparticles and recognize the local extrema in the pixel space. This technique successfully isolated the target location of the single molecule.

After optimization, polystyrene beads with known diameters were tested first to illustrate the power of this technology. The results show that this platform can successfully recognize and size individual polystyrene beads with diameters from 70 nm to 200 nm. Moreover, hundreds of H1N1 viruses were detected and sized in a single experiment (Daaboul et al., 2010). After proof of the concept utilizing polystyrene beads and H1N1 viruses, the platform was further modified for practical application (Fig. 9C-E). The substrate chip was first arrayed and functionalized with viruses-specific antibodies. Diluted wide-type vesicular stomatitis virus captured by these antibodies were identified with the LOD of 8×10^4 plaque-forming units/mL for both Ebola and Marburg VSV pseudotypes (Daaboul et al., 2014). This sensitivity is similar to or better than other antibody-based virus detection methods (Ksiazek et al., 1992; Towner et al., 2004), while the specificity and reproducibility of this sensor are also excellent.

3.4. Whole slide imaging for "digital" detection of single bacterium

The conventional light microscope is a powerful tool to detect tissues and cells qualitatively. The trade-off between the area of the FOV and the resolution of images hinders the conventional light microscope to be applied for quantitative analysis. However, the scanning function integrated with a conventional light microscope successfully bypasses this barrier. In 2019, a study took advantage of this technique to achieve real-time single analysis of viable bacteria at a single cell level and then use to determine the minimum inhibitory concentration and antibiotic susceptibility (Song et al., 2019).

The principle of this platform is illustrated in Fig. 10A-C. The prepared sample is inversely immobilized on the holder of the microscope. The scanning area of interest is selected using the software. During scanning, the stage where the sample is placed moves in a zigzag manner, and each autofocused FOV is imaged with a high resolution. A 30% overlap between adjacent images prevents any selected area from missing. Subsequent to the scanning, a built-in stitching function or commercialized software such as ImageJ can be employed to stitch individual images to a large image where the overlapping area can be eliminated. Thus, the number of target particles can be counted within individual images and the total number can be calculated. Because of the high resolution of each individual image, the activity of each particle such as the division of viable bacteria can be monitored and analyzed continuously by capturing images successively.

Particle immobilization and high transparency are two essential requirements for the sample that can be detected utilizing this platform. On one hand, the analysis can be ruined if particles to be imaged also moves concurrently because of the stage movement through imaging. On the other hand, low transparency can block the light to pass through the sample, thus interfering with imaging quality. In this study, a simple and cost-effective customized device was designed to meet these requirements (Song et al., 2018). A piece of thin Luria-Bertani (LB)-agarose gel film (0.38 mm) was employed for bacteria inoculation. It is easy to fabricate this thin film. Two pieces of microscope glass slides aligning vertically with two pieces of silica wafer inserted as spacers are placed in the Petri dish. Sterilized molten LB-agarose media is poured into the Petri dish and fills the space between two glass slides. Molten media solidifies as the temperature decrease. The gel on the bottom glass slide is ready for well-dispersed individual bacteria inoculation. A newly cleaned glass slide is tightly attached to the top of the gel inoculated with bacteria for particle immobilization. The advantage of replacing agar with agarose is to improve transparency for imaging. The highlight of this device is that it establishes an open system, and thus oxygen in the air is allowed to be diffused into the system to support bacteria growth (Fig. 10D and E), which allows the viable bacteria can be monitored in a real-time manner but with a relatively long time.
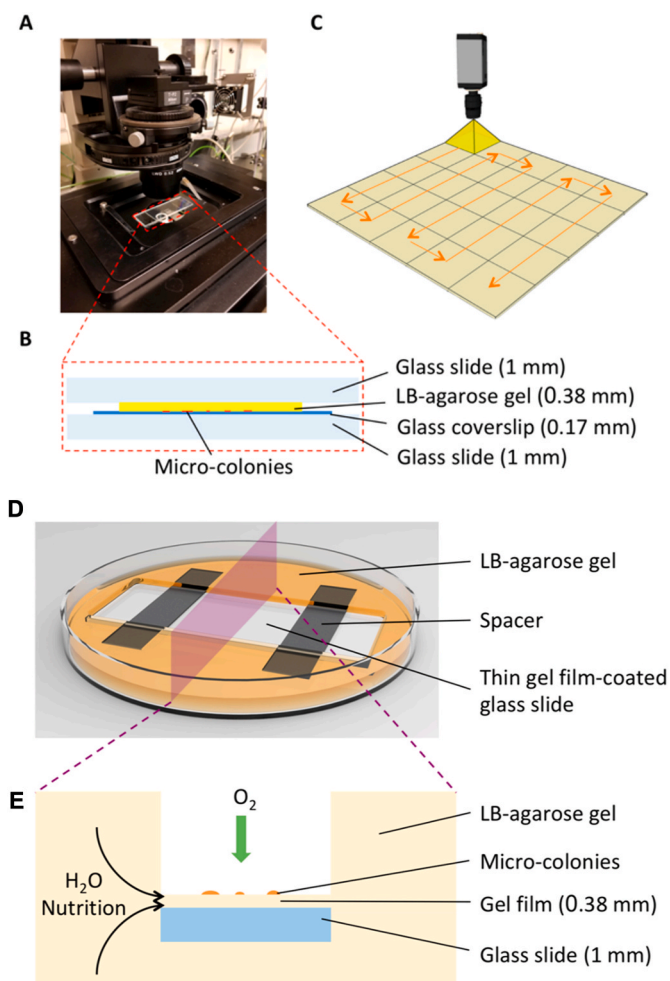

Fig. 10. (A) A photograph of the microscope with scanning function; (B) Side view of bacteria immobilization device; (C) Scheme of whole slide imaging in a zigzag manner. (D) Scheme of the customized device; (E) Side view of bacteria loaded gel film on the glass slide. Reprinted from (Song et al., 2018) under the Creative Commons Attribution 4.0 International License http://creativecommons.org/license s/by/4.0/.

Bacterial minimum inhibitory concentration and antibiotic susceptibility experiments were further conducted employing this platform by counting the individual viable and growth-inhibited (or dead) cells. To determine the minimum inhibitory concentration, individual division of *E. cloacae* in response to various concentrations of gentamicin was conducted. The minimum inhibitory concentration was 8 μg/mL. For antibiotic susceptibility test, kanamycin-resistant *E. coli* and susceptible *E. cloacae* cells coexist in the presence of 50 μg/mL of kanamycin were individually dispersed on the gel and used to screen antibiotic-resistant cells.

4. Nucleic acid amplification enabled "digital" detection

Nucleic acid has been always recognized as a unique biomarker for disease diagnosis. For example, the gold standard to diagnose COVID-19 is the reverse-transcription polymerase chain reaction (RT-PCR) test (Ai et al., 2020). Instead of being biomarker itself, nucleic acids can be replicated quickly and easily, enabling its detection through its amplification method as well as for other biomarkers. In this section, several recent studies have been summarized to introduce progress in the DNA-based amplification strategy within digital detection.

4.1. "Digital" PCR through compartment device

One foundation of digital polymerase chain reaction (dPCR) is the development of advanced devices that can compartmentalize sample solution into individual miniature chambers. Within the chamber, either one or zero DNA/RNA molecule can be distributed and amplified for generating the digital readout. Thus, to design tools and methods such as microchamber and microchannel is the trend in the initial development of dPCR.

A scalable self-priming fractal branching microchannel net chip is one of the most cutting-edge devices designed in 2017 (Zhu et al., 2017).

This chip is integrated with four layers, including an inlet layer, a waterproof layer, a microarray layer, and a glass coverslip from top to bottom accordingly (Fig. 11A). The inlet layer is a polydimethylsiloxane (PDMS) layer with four inlet holes for sample loading. The waterproof layer is inserted between the inlet layer and the microarray layer to prevent the evaporation of the sample solution. The microarray layer is where the PCR reaction occurs, which contains four reaction panels. Within each panel, there are 4096 individual microwells, resulting in that the total number of microwells is 16384 within one chip. The volume of each microwell is 5.625 nL. Glass coverslip enables the chip to be imaged utilizing a fluorescent microscope.
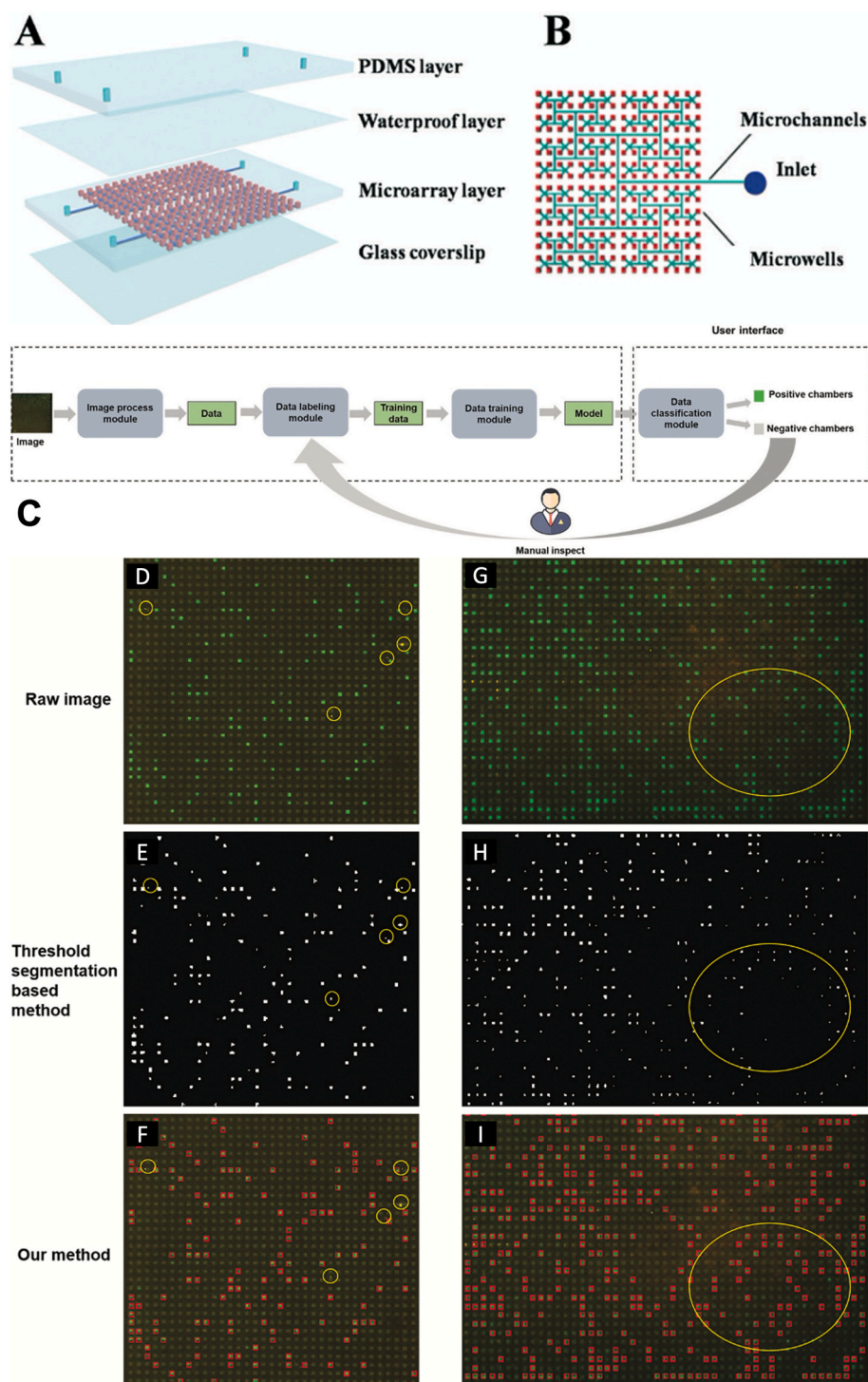

Fig. 11. (A) Scheme of the four layers chip; (B) Diagram of the microchannels design. Reprinted with permission from (Zhu et al., 2017). Copyright 2017 The Royal Society of Chemistry. (C) The workflow of the machine learning system. Comparison of traditional method and machine learning-based method. Yellow circles highlight the undesired fluorescent signal created by impurities in (D) raw image, image processed by (E) traditional method and (F) machine learning method. A large circle highlights the signals that are hard to recognize because of the unevenness of the images. Positive signals are ignored using (H) traditional method but recognized in the (I) machine learning method. (G) The raw image is displayed as a reference. Reprinted with permission from (Gou et al., 2019). Copyright 2019 The Royal Society of Chemistry. (For interpretation of the references to color in this figure legend, the reader is referred to the Web version of this article.)

Multiple intrinsic merits make this chip superior. The special design of fractal branching microchannel nets guarantees equal distance from the inlet to every individual microwell (Fig. 11B). The main channel is divided into two subchannels at one intersection. The subchannel continuously splits into two channels at the next intersection. All channels at ends are connected with four microwells. This branching strategy of sample solution compartmentalization facilitates the scalable process of the chip because the channels can be divided endlessly in theory. With the increment of the subchannels, more and more microwells can be created. However, the endless division may not be practical as the fluorescent signal from a too small volume of the microwell might be difficult to detect and the pressure drop is massive to cause flowing issues.

Another uniqueness of this chip is only one inlet without an outlet, which enables the self-priming reagent loading and avoids the loss of the sample. To compartmentalize the reagent into individual microwells, the chip with thousands of nanosized microwells was degassed and then been resumed to the atmosphere. The air can re-enter the chip, but this redissolution process will last for 4 h because of the miniature size of the microwell. Such pressure difference is the driving force for the reagent to be pushed into the microwells. At the same time, the long redissolution time allows reagents to be loaded or different reagents loading. For instance, after loading the sample, an immiscible reagent such as oil can be loaded to isolate the sample in each microwell and eliminate the cross-reaction. This self-priming reagent loading technique simplifies the sample loading and only a normal pipette is required to inject the sample solution, while the traditional methods rely on a syringe pump and require the operator to control the speed accurately. The self-priming loading technique also eliminates the sample loss because no solution can remain in the pathway to the dead-end microwell.

This chip was first applied to detect the copy number of DNA. 10^7 copies per μL of human β-actin DNA stock sample was prepared to validate this dPCR technique. The detection result was $(1.08 \pm 0.27) \times 10^7$ copies per μL, which is in good agreement with the expected value. Another application was for gene detection of low human hair follicle mesenchymal stem cell number. The regression curve was established to calculate the concentration of the target complementary DNA (cDNA). In 2018, this platform was successfully applied to detect the expression of marker genes of cancer stem-like cells, ALDH1A1, ABCG2, ALCAM, and CD133 within ALDH$^+$ A549 cells, ALDH$^-$ A549 cells and A549 cells (Xu et al., 2018).

After developing the original chip for sample compartmentalization, a machine learning-based strategy for data analysis was developed to discern positive wells from the background (Gou et al., 2019). Comparing to the conventional methods, this machine learning enabled new strategy further enhances accuracy and precision. Conventional methods complete the image segmentation using a single threshold determination which utilizes the pixel intensities difference between signal and background to find a proper threshold, but their reliability depends on the high uniformity of images. Therefore, the conventional methods cannot exclude the background noise whose fluorescence intensity is similar to the positive signal. Although the performance can be improved using the adaptive threshold method, it still cannot solve this problem fundamentally.

Instead of using conventional methods and their derivatives, the machine learning-based method can achieve a more accurate image analysis because of its unique feature. The strategy includes two steps, namely microwell positioning and signal classification. For the positioning step, the location of the microwells is determined according to the structure of the chip itself. This determination can focus on the area of interest precisely and physically ignore the undesired area such as the slits between microwells and the solution transfer channels, thus automatically eliminating the noise such as dust or any other fluorescent particles (Fig. 11D-F). For the classification step, the target microwell is not analyzed exclusively. As an opposite, surrounded microwells are collaborated to determine whether the analyzed one is positive, and thus

the analysis of each microwell is customized according to their feature, in conjunction with the surroundings to obtain the most reliable results. Another strategy to further improve reliability is the inclusion of manual inspection into the machine learning workflow (Fig. 11C). The results obtained based on the small amount of labeled training data are inspected by researchers. The corrected results are fitted to the existed training data set to form an iteration. Such iteration not only enhances the reliability of the results but also reduces the workload for researchers to label the original images. The performance of this new method is superior to traditional methods. Unrecognized positive microwells in the traditional methods can be easily recognized using this machine learning system and the detection accuracy reaches as high as 97.78% (Fig. 11G-I) (Gou et al., 2019).

4.2. dPCR through droplet partition

Another strategy to accomplish dPCR rather than employing a physical compartment device is to confine the bulk solution with all target molecules and PCR reagents into numerous droplets and then detect the signal within each droplet. The entire PCR process occurs within the droplets. Droplet dPCR has already been a mature technology and commercialized. The essential part of these commercialized instruments is the microfluidic system that can generate uniform small volume droplets. Recently, some pioneering studies support that droplet with specific volume is not indispensable at all (Byrnes et al., 2018a, 2018b; Yen et al., 2019). In 2020, a wash-free multiple volume droplet-based digital immunoassay was developed. The proximity ligation assay (PLA) was integrated as the signal amplification strategy (Byrnes et al., 2020).

Simple in-house multiple volume droplet generation is the most essential part of the method. The aqueous reaction contained antigen and PLA reagents is mixed with oil and then vortexed for 30 s, thus generating polydisperse water-in-oil droplets population. Through this partition, diameters of droplets are from 23.4 μm to 136.5 μm with an average of 31.3 μm. These droplets will contain several antigens, a single antigen, and no antigen for the following signal generation. The only instrument utilized in the droplet generation process is a vortex mixer. Comparing with the microfluidic system with a rigorous requirement for device fabrication and high cost, the vortex enabled droplet generation is apparently cost-effective and affordable.

PLA integrated qPCR signal amplification strategy is another important and innovative feature of this work. As target molecules, antigens, and PLA regents are partitioned into droplets, the PLA amplification process initiates within the droplets containing target molecules. A pair of oligo conjugated antibodies, a ligation oligo, a ligase, and DNA polymerase within each droplet are the components required for PLA (Fig. 12A). In the antigen containing droplets, two oligo conjugated antibodies bind to two epitopes on the same antigen. This binding event guarantees the two oligos conjugated on the two antibodies to be in close proximity, which allows the ligation oligo, a connector, and ligase to join with them and then form a closed circular DNA template. After subsequent quantitative polymerase chain reaction (qPCR) amplification and accumulation of amplified targets, positive droplets show an intensive fluorescence. For the droplets without antigens, no fluorescence signal can be detected because of a lack of adjacent oligo conjugated antibodies. Then both positive and negative droplets were transferred into a thin cell counting chamber for imaging. Images acquired by a fluorescent microscope were analyzed to identify positive droplets and conclude the concentration (Fig. 12C).

IL-8 was used as a representative antigen to evaluate the sensitivity of this method. The LOD is 6.61 pg/mL [95% CI: 4.95–9.27 pg/mL] (equivalent to 0.793 pM or 2.38×10^6 molecules) (Fig. 12B). Strictly speaking, this method is not a "true" single molecule detection method since there is no rigorous one-to-one correspondence between the target molecule and droplet. However, it has the potential to be optimized. For instance, increasing the ratio of droplets to target molecules and enable
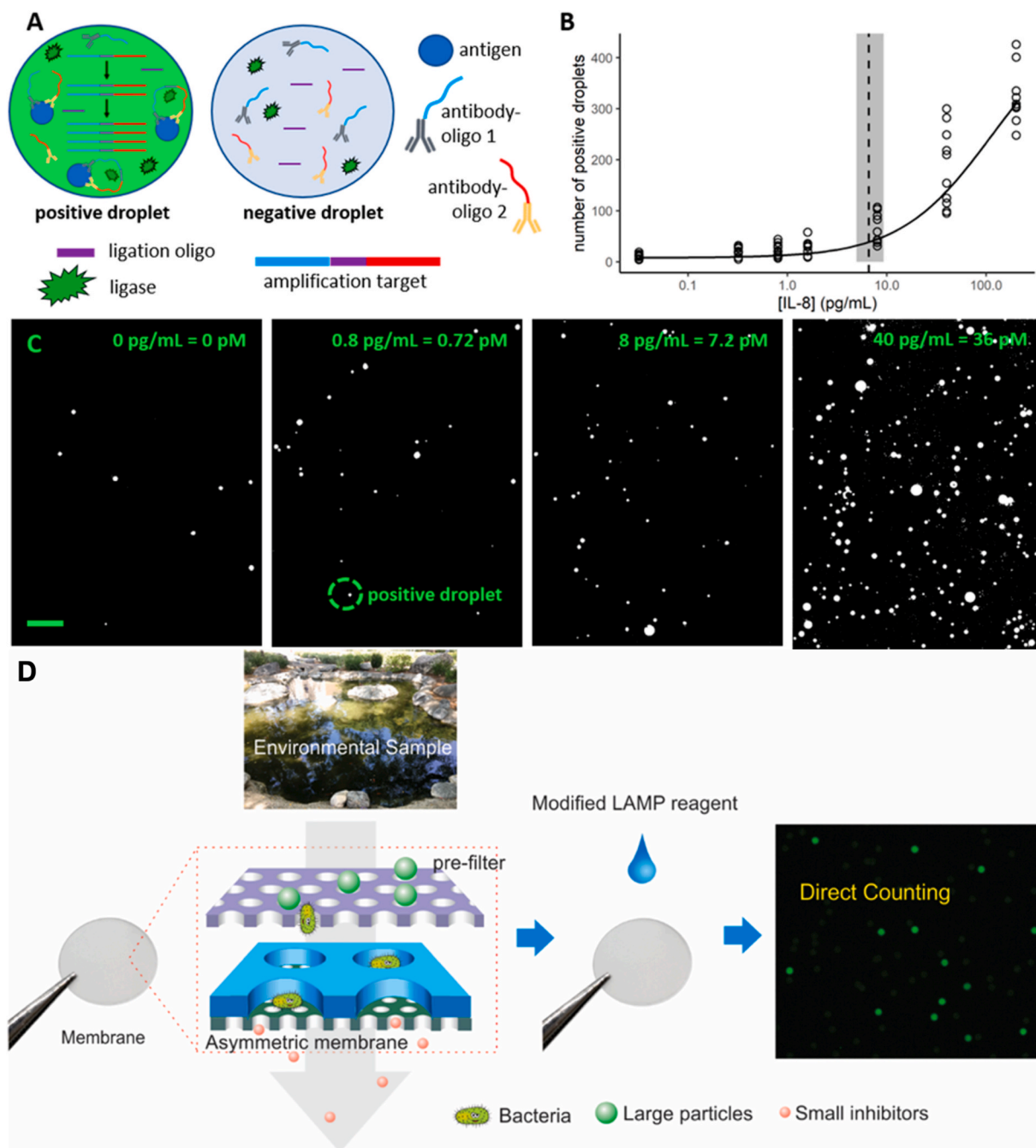
Fig. 12. (A) Scheme of PLA in positive and negative droplets; (B) IL-8 detection results; (C) Representative images of fluorescent images. Reprinted with permission from (Byrnes et al., 2020). Copyright 2020, American Chemical Society. (D) The scheme of the asymmetric system integrated with modified LAMP signal production. Reprinted with permission from (Lin et al., 2018). Copyright 2018 American Chemical Society.

the partition to follow the Poisson distribution.

4.3. Digital loop-mediated isothermal amplification (LAMP)

It is always highly demanded to develop new reliable, cost-effective, and fast detection methods of bacteria. The current gold standard method, culture-based colonies counting, is cumbersome and time-consuming. In 2018, a new platform utilizing an asymmetric membrane system with an integrated digital LAMP was developed to successfully detected bacteria in a digital manner (Lin et al, 2018, 2019).

The asymmetric membrane system and an adapted signal producing strategy based on the digital LAMP are the two highlights in this study. The principle that enabled this platform to accomplish the detection is

the size differentiation. As illustrated in Fig. 12D, the membrane system includes three commercially available polycarbonate (PC) membranes with varied pore sizes. The pre-filter membrane is a sacrificial track-etched PC membrane with negatively charged channel surface stacking on the top of the asymmetric membrane. It plays the role to exclude the undesired large granules and positive charged particles in the unprocessed environmental sample. The asymmetric membrane system includes two tightly attached PC membranes with the diameters of 25 μm for the top membrane and 400 nm for the bottom one. As the pre-filtered solution passing through, bacteria are trapped into the pore chambers of the top membrane, and soluble particles like proteins, metal ions, and organic compounds pass through to achieve purification. This purification process is crucial since some of these particles might be an

inhibitor to quench the LAMP reaction which is used to generate fluorescent signals for imaging.

LAMP is a relatively new technique that can amplify DNA under a constant temperature, which was developed in 2000 (Notomi et al., 2000). The main reason that LAMP was selected to produce the signal rather than mature PCR technology is that PCR requires temperature cycling (Thompson and Lei, 2020). For LAMP, the temperature is generally at 65 °C throughout the entire operation. However, directly using the standard LAMP generates false-negative results because of the release of inhibitor coming from bacterial lysates. To solve this problem, a calcein-Mn^{2+} indicator is introduced to amplify signals. Calcein is a soluble fluorescent dye with excitation and emission wavelengths of 495/515 nm. In the presence of Mn^{2+} in the solution, calcein-Mn^{2+} forms and calein's fluorescence is quenched. As the initiation of the LAMP, DNA of bacteria is amplified millions of times with the production of the byproduct, pyrophosphate, which reacts with Mn^{2+} to form precipitates and then calcein molecules are released and glow. Therefore, fluorescent pores in the membrane can be used as an indicator of the number of bacteria. One significant issue is the low efficiency of the standard LAMP without cell lysis because DNA is not released for amplification, which can be addressed using lysozyme with LAMP reagents.

Employing this platform, *E. coli* and *Salmonella* have been detected by spiking them into the unprocessed seawater and pond water. The dynamic range for *E. coli* in seawater is obtained from 0.3 to 10,000 cells/mL, while for *Salmonella* in pond water, it is 3–10,000 cells/mL.

There is a huge potential for this platform. The upmost one is affordable and cost-effective with the cost of 3 membranes less than 0.1 dollars. Also, there is no requirement of miscellaneous instruments such as a syringe pump, comparing with other similar methods. Moreover, no complicated sample preparation is required, and small bulk volume can be processed in a few seconds. All these features make it a powerful platform in digital diagnosis.

5. Conclusion and future trends

High-performance single-molecule detection with high sensitivity, accuracy, and precision will enhance the ability of human beings to fight diseases and secure food safety. Up to date, antibody-antigen binding based immunoassay and nucleic acid detection are still the two mainstream methods to accomplish the detection of biomolecules because of specificity of antibody-antigen recognition and the uniqueness of nucleic acid sequence.

Employing a surrogate signal development system has been the mainstream in the development of digital immunoassays, but the use of digital visualization or discovery of new methods has also been undergoing. The small size of most biomolecules of interest is a major obstacle interfering with the detection. The principle of using surrogate signal development is to enable the complex containing target molecules to produce a distinguishable signal, compared with the other entities as well as background. To achieve digital counting, the widely employed colorimetric method must be integrated with a compartment system for single particle detection since the analog signal must be confined to maintain a one-to-one correspondence between the target molecule and signal. On the other hand, introducing bead-based or fluorophores conjugated strategy can avoid the need of partition in some cases, but there are some rigorous requirements including that the fluorescence displayed by the fluorophores conjugated detection antibody must be intensive enough to be measured; the size of the beads conjugated on the immunocomplex must be proper and distinguishable, and also not damage the weak antibody-antigen binding. Comparing to the digital detection enabled by surrogate signal development strategies, digital visualization such as SPRi and BPM are simple and direct, but they usually have a high requirement for instruments, which is usually not accessible or unaffordable.

To achieve partition in digital detection, the microfluidic system is a critical part of sample compartmentalization (Leirs et al., 2016; Witters et al., 2013), but the non-compartmentalized system is now developed as well. It is a mature and reliable technology to employing a microfluidic system to develop uniform small chambers on a substrate or generate droplets, whose advantages lie on the excellent repeatability and miniature size of the device. Nevertheless, this technique is always tedious in manufacturing. Generation of master mask and microfabrication of devices are expensive and requires advanced facilities. Also, a syringe pump and specific tubing are usually in need to complete the experimental set. All these limitations stimulate researchers to develop alternative methods. Up to date, plenty of detection platforms have been developed including the aforementioned reporter elution system.

To develop digital detection of biomolecules with single copy sensitivity is a multidisciplinary research, which requires an integration of different strategies, advanced instruments, and interdisciplinary collaboration. One simple way to improve the performance in digital detection is to combine existing strategies to develop a new platform by taking their advantages while avoiding their limitations. Several successful stories have been summarized in previous sections. In the aforementioned BPM study, the switch of particle mobility is a new signal which is detectable to achieve single particle activity monitoring. However, only several hundred activities can be monitored at the same time, which prevents this technique from concentration determination in a counting manner. Recently, a study successfully confined a single tethered molecule in a small chamber to monitor its mobility switch and determine the concentration of PSA, which offers a new avenue to expand the application of existing methods (Akama et al., 2019a). Also, enormous methods cannot be further improved purely because of the limitation by the resolution of current instruments. For instance, a fluorescent microscope is a powerful tool for detection but barely applied in digital detection due to the small FOV. It is difficult to acquire the entire area of interest in high quality. Although some solutions have emerged, the improvement is inadequate. For instance, lens-free techniques are a substitute for the conventional light microscope. However, to obtain large FOV sacrifices the resolution of images (Cermak et al., 2016). Such obstacles can be easily addressed by integrating scanning function into various light microscopes. The aforementioned whole slide imaging or scanning method exploits this function to accomplish bacteria detection easily. It can also be extended to the detection of protein biomarker and nucleic acid which is under development in our lab. Another trend in digital diagnosis is to integrate machine learning into image process and counting criteria, thus offering a huge potential to improve the accuracy and other analytical characteristics (Esteva et al., 2017; Jordan and Mitchell, 2015; Ren et al., 2018; Sendek et al., 2017; Ulissi et al., 2017; Zhang et al., 2017; Zhou et al., 2018). Pioneering research integrating machine learning into dPCR research for data process which was discussed in the previous section will lead this trend toward molecule detection fields. We strongly believe that with the progress of science and technology, more reliable and user-friendly digital sensing platforms will be developed and commercialized in the near future and impact our community with unprecedented power.

Author contributions

The manuscript was written through contributions of all authors. All authors have given approval to the final version of the manuscript.

CRediT authorship contribution statement

Haomin Liu: Writing - original draft. **Yu Lei:** Writing - review & editing.

Declaration of competing interest

The authors declare that they have no known competing financial

Acknowledgements

References

Ai, T., Yang, Z., Hou, H., Zhan, C., Chen, C., Lv, W., Tao, Q., Sun, Z., Xia, L., 2020. Correlation of chest CT and RT-PCR testing in coronavirus disease 2019 (COVID-19) in China: a report of 1014 cases. Radiology 200642.

Akama, K, Iwanaga, N, Yamawaki, K, Okuda, M, Jain, K, Ueno, H, Soga, N, Minagawa, Y, Noji, H, 2019a. Wash-and amplification-free digital immunoassay based on single-particle motion analysis. ACS Nano. 113 (11), 13116–13126. https://doi.org/10.1021/acsnano.9b05917.

Akama, K., Shirai, K., Suzuki, S., 2019b. Highly sensitive multiplex protein detection by droplet-free digital ELISA. Electron. Commun. Jpn. 102, 43–47. https://doi.org/10.1002/ecj.12137.

Akama, K., Shirai, K., Suzuki, S., 2016. Droplet-free digital enzyme-linked immunosorbent assay based on a tyramide signal amplification system. Anal. Chem. 88, 7123–7129. https://doi.org/10.1021/acs.analchem.6b01148.

Baker, C.A., Duong, C.T., Grimley, A., Roper, M.G., 2009. Recent advances in microfluidic detection systems. Bioanalysis 1, 967–975.

Barletta, J.M., Edelman, D.C., Constantine, N.T., 2004. Lowering the detection limits of HIV-1 viral load using real-time immuno-PCR for HIV-1 p24 antigen. Am. J. Clin. Pathol. 122, 20–27.

Bohren, C.F., Huffman, D.R., 2008. Absorption and Scattering of Light by Small Particles. John Wiley & Sons.

Byrnes, S.A., Chang, T.C., Huynh, T., Astashkina, A., Weigl, B.H., Nichols, K.P., 2018a. Simple polydisperse droplet emulsion polymerase chain reaction with statistical volumetric correction compared with microfluidic droplet digital polymerase chain reaction. Anal. Chem. 90, 9374–9380. https://doi.org/10.1021/acs.analchem.8b01988.

Byrnes, S.A., Huynh, T., Chang, T.C., Anderson, C.E., McDermott, J.J., Oncina, C.I., Weigl, B.H., Nichols, K.P., 2020. Wash-free, digital immunoassay in polydisperse droplets. Anal. Chem. 92, 3535–3543. https://doi.org/10.1021/acs.analchem.9b02526.

Byrnes, S.A., Phillips, E.A., Huynh, T., Weigl, B.H., Nichols, K.P., 2018b. Polydisperse emulsion digital assay to enhance time to detection and extend dynamic range in bacterial cultures enabled by a statistical framework. Analyst 143, 2828–2836. https://doi.org/10.1039/c8an00029h.

Cermak, N., Olcum, S., Delgado, F.F., Wasserman, S.C., Payer, K.R., A Murakami, M., Knudsen, S.M., Kimmerling, R.J., Stevens, M.M., Kikuchi, Y., Sandikci, A., Ogawa, M., Agache, V., Baléras, F., Weinstock, D.M., Manalis, S.R., 2016. High-throughput measurement of single-cell growth rates using serial microfluidic mass sensor arrays. Nat. Biotechnol. 34, 1052–1059. https://doi.org/10.1038/nbt.3666.

Chang, L., Rissin, D.M., Fournier, D.R., Piech, T., Patel, P.P., Wilson, D.H., Duffy, D.C., 2012. Single molecule enzyme-linked immunosorbent assays: theoretical considerations. J. Immunol. Methods 378, 102–115. https://doi.org/10.1016/j.jim.2012.02.011.

Daaboul, G.G., Lopez, C.A., Chinnala, J., Goldberg, B.B., Connor, J.H., Selim Ünlü, M., 2014. Digital sensing and sizing of vesicular stomatitis virus pseudotypes in complex media: a model for ebola and marburg detection. ACS Nano 8, 6047–6055. https://doi.org/10.1021/nn501312q.

Daaboul, G.G., Yurt, A., Zhang, X., Hwang, G.M., Goldberg, B.B., Ünlü, M.S., 2010. High-throughput detection and sizing of individual low-index nanoparticles and viruses for pathogen identification. Nano Lett. 10, 4727–4731. https://doi.org/10.1021/nl103210p.

Dinh, T.L., Ngan, K.C., Shoemaker, C.B., Walt, D.R., 2016. Using antigen–antibody binding kinetic parameters to understand single-molecule array immunoassay performance. Anal. Chem. 88 (23), 11335–11339. https://doi.org/10.1021/acs.analchem.6b03192.

Eastwood, K., Else, P., Charlett, A., Wilcox, M., 2009. Comparison of nine commercially available Clostridium difficile toxin detection assays, a real-time PCR assay for C. difficile tcdB, and a glutamate dehydrogenase detection assay to cytotoxin testing and cytotoxigenic culture methods. J. Clin. Microbiol. 47, 3211–3217. https://doi.org/10.1128/JCM.01082-09.

Esteva, A., Kuprel, B., Novoa, R.A., Ko, J., Swetter, S.M., Blau, H.M., Thrun, S., 2017. Dermatologist-level classification of skin cancer with deep neural networks. Nature 542, 115–118. https://doi.org/10.1038/nature21056.

Gally, D.L., Stevens, M.P., 2017. Microbe profile: Escherichia coli O157: H7 – notorious relative of the microbiologist's workhorse. Microbiol. 163, 1–3. https://doi.org/10.1099/mic.0.000387.

Gaylord, S.T., Abdul-Aziz, S., Walt, D.R., 2015a. Single-molecule arrays for ultrasensitive detection of host immune response to dengue virus infection. J. Clin. Microbiol. 53 (5), 1722–1724. https://doi.org/10.1128/JCM.03487-14.

Gaylord, S.T., Dinh, T.L., Goldman, E.R., Anderson, G.P., Ngan, K.C., Walt, D.R., 2015b. Ultrasensitive detection of ricin toxin in multiple sample matrixes using single-domain antibodies. Anal. chem. 87 (13), 6570–6577. https://doi.org/10.1021/acs.analchem.5b00322.

Giljohann, D.A., Mirkin, C.A., 2009. Drivers of biodiagnostic development. Nature 462, 461.

Gite, S., Archambault, D., Cappillino, M.P., Cunha, D., Dorich, V., Shatova, T., Tempesta, A., Walsh, B., Walsh, J.A., Williams, A., Kirby, J.E., Bowers, J., Straus, D., 2018. A rapid, accurate, single molecule counting method detects Clostridium difficile toxin B in stool samples. Sci. Rep. 8, 8364. https://doi.org/10.1038/s41598-018-26353-0.

Gou, T., Hu, J., Zhou, S., Wu, W., Fang, W., Sun, J., Hu, Z., Shen, H., Mu, Y., 2019. A new method using machine learning for automated image analysis applied to chip-based digital assays. Analyst 144, 3274–3281. https://doi.org/10.1039/c9an00149b.

Hennequin, Y., Allier, C.P., McLeod, E., Mudanyali, O., Migliozzi, D., Ozcan, A., Dinten, J.M., 2013. Optical detection and sizing of single nanoparticles using continuous wetting films. ACS Nano 7, 7601–7609. https://doi.org/10.1021/nn403431y.

Higuchi, R., Fockler, C., Dollinger, G., Watson, R., 1993. Kinetic PCR analysis: real-time monitoring of DNA amplification reactions. Bio Technol. 11, 1026–1030. https://doi.org/10.1038/nbt0993-1026.

Huang, B., Yu, F., Zare, R.N., 2007. Surface plasmon resonance imaging using a high numerical aperture microscope objective. Anal. Chem. 79, 2979–2983. https://doi.org/10.1021/ac062284x.

Janelidze, S., Stomrud, E., Palmqvist, S., Zetterberg, H., van Westen, D., Jeromin, A., Song, L., Hanlon, D., Tan Hehir, C.A., Baker, D., Blennow, K., Hansson, O., 2016. Plasma β-amyloid in Alzheimer's disease and vascular disease. Sci. reports 6 (1), 1–11. https://doi.org/10.1038/srep26801.

January, F., Hospital, T., Hospital, T., January, E., Bacteria, A., Travelers, I., Myotomy, S., Chronic, R., Leukemia, M., Allergy, P., Thrombosis, V., Ap, S., Seafood, H., Market, W., 2020. Correspondence Detection of Covid-19 in Children in Early January 2020 in Wuhan (China).

Jordan, M.I., Mitchell, T.M., 2015. Machine learning: trends, perspectives, and prospects. Science 349 (80), 255–260. https://doi.org/10.1126/science.aaa8415.

Kan, C.W., Rivnak, A.J., Campbell, T.G., Piech, T., Rissin, D.M., Mösl, M., Petera, A., Niederberger, H.P., Minnehan, K.A., Patel, P.P., Ferrell, E.P., Meyer, R.E., Chang, L., Wilson, D.H., Fournier, D.R., Duffy, D.C., 2012. Isolation and detection of single molecules on paramagnetic beads using sequential fluid flows in microfabricated polymer array assemblies. Lab Chip 12, 977–985. https://doi.org/10.1039/c2lc20744c.

Kan, C.W., Tobos, C.I., Rissin, D.M., Wiener, A.D., Meyer, R.E., Svancara, D.M., Comperchio, A., Warwick, C., Millington, R., Collier, N., Duffy, D.C., 2020. Digital enzyme-linked immunosorbent assays with sub-attomolar detection limits based on low numbers of capture beads combined with high efficiency bead analysis. Lab Chip (12). https://doi.org/10.1039/d0lc00267d.

Karch, H., Tarr, P.I., Bielaszewska, M., 2005. Enterohaemorrhagic Escherichia coli in human medicine. Int. J. Med. Microbiol. 295, 405–418. https://doi.org/10.1016/j.ijmm.2005.06.009.

Khalil, M., Pirpamer, L., Hofer, E., Voortman, M.M., Barro, C., Leppert, D., Benkert, P., Ropele, S., Enzinger, C., Fazekas, F., Schmidt, R., Kuhle, J., 2020. Serum neurofilament light levels in normal aging and their association with morphologic brain changes. Nat. Commun. 11 (1) https://doi.org/10.1038/s41467-020-14612-6.

Ksiazek, T.G., Rollin, P.E., Jahrling, P.B., Johnson, E., Dalgard, D.W., Peters, C.J., 1992. Enzyme immunosorbent assay for Ebola virus antigens in tissues of infected primates. J. Clin. Microbiol. 30, 947–950.

Leirs, K., Tewari Kumar, P., Decrop, D., Pérez-Ruiz, E., Leblebici, P., Van Kelst, B., Compernolle, G., Meeuws, H., Van Wesenbeeck, L., Lagatie, O., Stuyver, L., Gils, A., Lammertyn, J., Spasic, D., 2016. Bioassay development for ultrasensitive detection of influenza A nucleoprotein using digital ELISA. Anal. Chem. 88, 8450–8458. https://doi.org/10.1021/acs.analchem.6b00502.

Lin, X., Huang, X., Urmann, K., Xie, X., Hoffmann, M.R., 2019. Digital loop-mediated isothermal amplification on a commercial membrane. ACS Sens. 4, 242–249. https://doi.org/10.1021/acssensors.8b01419.

Lin, X., Huang, X., Zhu, Y., Urmann, K., Xie, X., Hoffmann, M.R., 2018. Asymmetric membrane for digital detection of single bacteria in milliliters of complex water samples. ACS Nano. 12 (10), 10281–10290. https://doi.org/10.1021/acsnano.8b05384.

Long, Q.-X., Liu, B.-Z., Deng, H.-J., Wu, G.-C., Deng, K., Chen, Y.-K., Liao, P., Qiu, J.-F., Lin, Y., Cai, X.-F., Wang, D.-Q., Hu, Y., Ren, J.-H., Tang, N., Xu, Y.-Y., Yu, L.-H., Mo, Z., Gong, F., Zhang, X.-L., Tian, W.-G., Hu, L., Zhang, X.-X., Xiang, J.-L., Du, H.-X., Liu, H.-W., Lang, C.-H., Luo, X.-H., Wu, S.-B., Cui, X.-P., Zhou, Z., Zhu, M.-M., Wang, J., Xue, C.-J., Li, X.-F., Wang, L., Li, Z.-J., Wang, K., Niu, C.-C., Yang, Q.-J., Tang, X.-J., Zhang, Y., Liu, X.-M., Li, J.-J., Zhang, D.-C., Zhang, F., Liu, P., Yuan, J., Li, Q., Hu, J.-L., Chen, J., Huang, A.-L., 2020. Antibody responses to SARS-CoV-2 in patients with COVID-19. Nat. Med. 1–4. https://doi.org/10.1038/s41591-020-0897-1.

Monroe, M.R., Daaboul, G.G., Tuysuzoglu, A., Lopez, C.A., Little, F.F., Ünlü, M.S., 2013. Single nanoparticle detection for multiplexed protein diagnostics with attomolar sensitivity in serum and unprocessed whole blood. Anal. Chem. 85, 3698–3706. https://doi.org/10.1021/ac4000514.

Nie, S., Henley, W.H., Miller, S.E., Zhang, H., Mayer, K.M., Dennis, P.J., Oblath, E.A., Alarie, J.P., Wu, Y., Oppenheim, F.G., Little, F.F., Uluer, A.Z., Wang, P., Ramsey, J. M., Walt, D.R., 2014. An automated integrated platform for rapid and sensitive

multiplexed protein profiling using human saliva samples. Lab Chip 14, 1087–1098. https://doi.org/10.1039/c3lc51303c.

Notomi, T., Okayama, H., Masubuchi, H., Yonekawa, T., Watanabe, K., Amino, N., Hase, T., 2000. Loop-mediated isothermal amplification of DNA. Nucleic Acids Res. 28 https://doi.org/10.1093/nar/28.12.e63 e63–e63.

O'Connell, G.C., Alder, M.L., Smothers, C.G., Still, C.H., Webel, A.R., Moore, S.M., 2020. Use of high-sensitivity digital ELISA improves the diagnostic performance of circulating brain-specific proteins for detection of traumatic brain injury during triage. Neurol. Res. 42, 346–353. https://doi.org/10.1080/01616412.2020.1726588.

Phillips, K.S., Wilkop, T., Wu, J.-J., Al-Kaysi, R.O., Cheng, Q., 2006. Surface plasmon resonance imaging analysis of protein-receptor binding in supported membrane arrays on gold substrates with calcinated silicate films. J. Am. Chem. Soc. 128, 9590–9591. https://doi.org/10.1021/ja0628102.

Pollock, N.R., Song, L., Zhao, M., Duffy, D.C., Chen, X., Sambol, S.P., Gerding, D.N., Kelly, C.P., 2015. Differential immunodetection of toxin B from highly virulent Clostridium difficile BI/NAP-1/027. J. Clin. Microbiol. 53, 1705–1708. https://doi.org/10.1128/JCM.03419-14.

Reddington, A.P., Trueb, J.T., Freedman, D.S., Tuysuzoglu, A., Daaboul, G.G., Lopez, C.A., Karl, W.C., Connor, J.H., Fawcett, H., Unlu, M.S., 2013. An interferometric reflectance imaging sensor for point of care viral diagnostics. IEEE Trans. Biomed. Eng. 60, 3276–3283. https://doi.org/10.1109/TBME.2013.2272666.

Ren, F., Ward, L., Williams, T., Laws, K.J., Wolverton, C., Hattrick-Simpers, J., Mehta, A., 2018. Accelerated discovery of metallic glasses through iteration of machine learning and high-throughput experiments. Sci. Adv. 4 https://doi.org/10.1126/sciadv.aaq1566.

Rissin, D.M., Kan, C.W., Campbell, T.G., Howes, S.C., Fournier, D.R., Song, L., Piech, T., Patel, P.P., Chang, L., Rivnak, A.J., Ferrell, E.P., Randall, J.D., Provuncher, G.K., Walt, D.R., Duffy, D.C., 2010. Single-molecule enzyme-linked immunosorbent assay detects serum proteins at subfemtomolar concentrations. Nat. Biotechnol. 28, 595–599. https://doi.org/10.1038/nbt.1641.

Rissin, D.M., Kan, C.W., Song, L., Rivnak, A.J., Fishburn, M.W., Shao, Q., Fournier, D.R., 2013a. Multiplexed single molecule immunoassays. Lab Chip 13 (15), 2902–2911. https://doi.org/10.1039/c3lc50416f.

Rissin, D.M., Wilson, D.H., Duffy, D.C., 2013b. In: Wild, D.B.T.T.I.H., Fourth, E. (Eds.), Chapter 2.13 - Measurement of Single Protein Molecules Using Digital ELISA. Elsevier, Oxford, pp. 223–242. https://doi.org/10.1016/B978-0-08-097037-0.00016-6.

Rivnak, A.J., Rissin, D.M., Kan, C.W., Song, L., Fishburn, M.W., Piech, T., Campbell, T.G., DuPont, D.R., Gardel, M., Sullivan, S., Pink, B.A., Cabrera, C.G., Fournier, D.R., Duffy, D.C., 2015. A fully-automated, six-plex single molecule immunoassay for measuring cytokines in blood. J. Immunol. Methods 424, 20–27. https://doi.org/10.1016/j.jim.2015.04.017.

Rothenhäusler, B., Knoll, W., 1988. Surface–plasmon microscopy. Nature 332, 615–617. https://doi.org/10.1038/332615a0.

Sakamoto, C., Yamaguchi, N., Nasu, M., 2005. Rapid and simple quantification of bacterial cells by using a microfluidic device. Appl. Environ. Microbiol. 71, 1117–1121. https://doi.org/10.1128/AEM.71.2.1117-1121.2005.

Schleifer, K.H., Kloos, W.E., 1975. Isolation and characterization of Staphylococci from human skin I. Amended descriptions of Staphylococcus epidermidis and Staphylococcus saprophyticus and descriptions of three new species: Staphylococcus cohnii, Staphylococcus haemolyticus, and Staphyloc. Int. J. Syst. Evol. Microbiol. 25, 50–61.

Sendek, A.D., Yang, Q., Cubuk, E.D., Duerloo, K.A.N., Cui, Y., Reed, E.J., 2017. Holistic computational structure screening of more than 12 000 candidates for solid lithium-ion conductor materials. Energy Environ. Sci. 10, 306–320. https://doi.org/10.1039/c6ee02697d.

Shim, J.U., Ranasinghe, R.T., Smith, C.A., Ibrahim, S.M., Hollfelder, F., Huck, W.T.S., Klenerman, D., Abell, C., 2013. Ultrarapid generation of femtoliter microfluidic droplets for single-molecule-counting immunoassays. ACS Nano 7, 5955–5964. https://doi.org/10.1021/nn401661d.

Shumaker-Parry, J.S., Zareie, M.H., Aebersold, R., Campbell, C.T., 2004. Microspotting streptavidin and double-stranded DNA arrays on gold for high-throughput studies of Protein−DNA interactions by surface plasmon resonance microscopy. Anal. Chem. 76, 918–929. https://doi.org/10.1021/ac034964v.

Son, J., Hwang, J., Lee, D., Khan, M.S., Jo, Y., Lee, K., Park, C., Chavan, S., Seo, Y., Choi, Y., Kim, S., Kim, D., Na, D., Choi, J., 2018. Strategies for the optimization of bead-immunoassays for the effective detection of target biomolecules. Kor. J. Chem. Eng. 35, 805–811. https://doi.org/10.1007/s11814-017-0323-7.

Song, D., Liu, H., Dong, Q., Bian, Z., Wu, H., Lei, Y., 2018. Digital, rapid, accurate, and label-free enumeration of viable microorganisms enabled by custom-built on-glass-slide culturing device and microscopic scanning. Sensors 18. https://doi.org/10.3390/s18113700.

Song, D., Liu, H., Ji, H., Lei, Y., 2019. Whole slide imaging for high-throughput sensing antibiotic resistance at single-bacterium level and its application to rapid antibiotic susceptibility testing. Molecules 24. https://doi.org/10.3390/molecules24132441.

Song, L., Shan, D., Zhao, M., Pink, B.A., Minnehan, K.A., York, L., Gardel, M., Sullivan, S., Phillips, A.F., Hayman, R.B., Walt, D.R., Duffy, D.C., 2013. Direct detection of bacterial genomic DNA at sub-femtomolar concentrations using single molecule arrays. Anal. Chem. 85, 1932–1939. https://doi.org/10.1021/ac303426b.

Thompson, D., Lei, Y., 2020. Mini review: recent progress in RT-LAMP enabled COVID-19 detection. Sensor. Actuator. Rep. 2, 100017. https://doi.org/10.1016/j.snr.2020.100017.

Towner, J.S., Rollin, P.E., Bausch, D.G., Sanchez, A., Crary, S.M., Vincent, M., Lee, W.F., Spiropoulou, C.F., Ksiazek, T.G., Lukwiya, M., Kaducu, F., Downing, R., Nichol, S.T., 2004. Rapid diagnosis of ebola hemorrhagic fever by reverse transcription-PCR in an outbreak setting and assessment of patient viral load as a predictor of outcome. J. Virol. 78, 4330–4341. https://doi.org/10.1128/JVI.78.8.4330-4341.2004.

Ulissi, Z.W., Medford, A.J., Bligaard, T., Nørskov, J.K., 2017. To address surface reaction network complexity using scaling relations machine learning and DFT calculations. Nat. Commun. 8, 1–7. https://doi.org/10.1038/ncomms14621.

Visser, E.W.A., Yan, J., Van IJzendoorn, L.J., Prins, M.W.J., 2018. Continuous biomarker monitoring by particle mobility sensing with single molecule resolution. Nat. Commun. 9, 1–10. https://doi.org/10.1038/s41467-018-04802-8.

Vo-Dinh, T., Mahadevan-Jansen, A., Grundfest, W.S., McGuigan, W., Fournier, D.R., Watson, G.W., Walling, L., Gigante, B., Duffy, D.C., Rissin, D.M., Kan, C.W., Meyer, R.E., Piech, T., Fishburn, M.W., 2014. The optics inside an automated single molecule array analyzer. Adv. Biomed. Clin. Diagnostic Syst. XII https://doi.org/10.1117/12.2041706.

Wang, S., Shan, X., Patel, U., Huang, X., Lu, J., Li, J., Tao, N., 2010. Label-free imaging, detection, and mass measurement of single viruses by surface plasmon resonance. Proc. Natl. Acad. Sci. U. S. A 107, 16028–16032. https://doi.org/10.1073/pnas.1005264107.

Wang, X., Cohen, L., Wang, J., Walt, D.R., 2018. Competitive immunoassays for the detection of small molecules using single molecule arrays. J. Am. Chem. Soc. 140, 18132–18139. https://doi.org/10.1021/jacs.8b11185.

Witters, D., Knez, K., Ceyssens, F., Puers, R., Lammertyn, J., 2013. Digital microfluidics-enabled single-molecule detection by printing and sealing single magnetic beads in femtoliter droplets. Lab Chip 13, 2047–2054. https://doi.org/10.1039/c3lc50119a.

Wu, D., Milutinovic, M.D., Walt, D.R., 2015. Single molecule array (Simoa) assay with optimal antibody pairs for cytokine detection in human serum samples. Analyst 140 (18), 6277–6282. https://doi.org/10.1039/c5an01238d.

Xu, Y., Hu, J., Zhu, Q., Song, Q., Mu, Y., 2018. Co-detection of ALDH1A1, ABCG2, ALCAM and CD133 in three A549 subpopulations at the single cell level by one-step digital RT-PCR. Integr. Biol. (United Kingdom) 10, 364–369. https://doi.org/10.1039/c8ib00042e.

Yan, Z.-H., Zhang, W., Rollins, N., Tayber, O., Chen, J., Wu, D., Brauer, P., Chouitar, J., Bosse, R., Yu, J., Bembenek, M.E., 2016. An ultrasensitive assay format for detecting ULK1 inhibition by monitoring the phosphorylation status of Atg 13. Anal. Biochem. 509, 73–78. https://doi.org/10.1016/j.ab.2016.06.023.

Yen, G.S., Fujimoto, B.S., Schneider, T., Kreutz, J.E., Chiu, D.T., 2019. Statistical analysis of nonuniform volume distributions for droplet-based digital PCR assays. J. Am. Chem. Soc. 141, 1515–1525. https://doi.org/10.1021/jacs.8b09073.

Zhang, J., Lu, S., Wang, X., Du, X., Ni, G., Liu, J., Liu, L., Liu, Y., 2017. Automatic identification of fungi in microscopic leucorrhea images. J. Opt. Soc. Am. A 34, 1484. https://doi.org/10.1364/josaa.34.001484.

Zhang, Q., Zhang, X., Li, J., Gai, H., 2020. Nonstochastic protein counting analysis for precision biomarker detection: suppressing Poisson noise at ultralow concentration. Anal. Chem. 92, 654–658. https://doi.org/10.1021/acs.analchem.9b04809.

Zhou, Q., Tang, P., Liu, S., Pan, J., Yan, Q., Zhang, S.C., 2018. Learning atoms for materials discovery. Proc. Natl. Acad. Sci. U. S. A 115, E6411–E6417. https://doi.org/10.1073/pnas.1801181115.

Zhou, X., Yang, Y., Wang, S., Liu, X., 2020. Surface plasmon resonance microscopy: from single-molecule sensing to single-cell imaging. Angew. Chem. 132, 1792–1801. https://doi.org/10.1002/ange.201908806.

Zhu, Q., Xu, Y., Qiu, L., Ma, C., Yu, B., Song, Q., Jin, W., Jin, Q., Liu, J., Mu, Y., 2017. A scalable self-priming fractal branching microchannel net chip for digital PCR. Lab Chip 17, 1655–1665. https://doi.org/10.1039/c7lc00267j.